Effects of X ray Edge In the Ptolemy Project

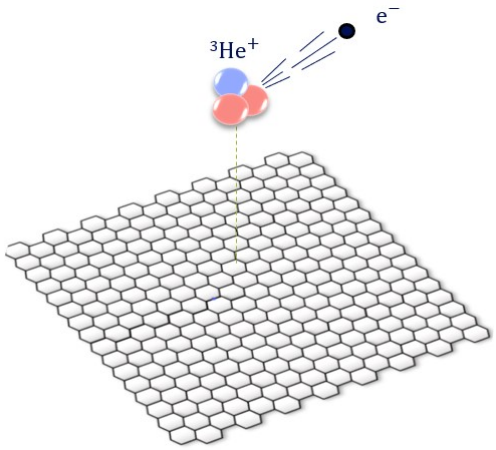

THESIS

submitted in partial fulfillment of the
requirements for the degree of

MASTER OF SCIENCE
in
RESEARCH IN THEORETICAL PHYSICS

Author :	Zhiyang Tan
Student ID :	s2552973
Supervisor :	Dr. Vadim Cheianov
Second corrector :	Dr. Alexey Boyarsky

Leiden, The Netherlands, July 12, 2021

Effects of X ray Edge In the Ptolemy Project

Zhiyang Tan

Huygens-Kamerlingh Onnes Laboratory, Leiden University
P.O. Box 9500, 2300 RA Leiden, The Netherlands

July 12, 2021

Abstract

Cosmic neutrino background (CνB) has long stimulated astronomers' interest since it contains the information of the universe 1 second after the Big Bang. Recently, the Ptolemy project was proposed to detect the CνB directly. It uses graphene to localize the tritium atoms to provide a very high energy resolution. Still, it pays a price of spectrum broadening due to the interaction between graphene and tritium atoms. In this paper, we presented how the X-ray edge influences the Ptolemy project. We found out that the smeared beta decay spectrum is the convolution between the spectral density function of graphene and the original beta decay spectrum. Using the linked cluster expansion, we obtain the spectral density function of graphene, precisely the gamma distribution function, and controlled by two parameters, the coupling constant and the cutoff energy. Moreover, we also investigated factors that influence the coupling constant and the cutoff energy. We found out that dynamic screening effects change the coupling constant significantly for the freestanding graphene. Still, we can rule the disorder effects out if the tritium concentration is below $5 \times 10^{11}/\mathrm{cm}^2$. In the end, we developed the determinant method to obtain a more rigorous dependence of the coupling constant on the external dielectric constant for the graphene deposited on a low-dielectric-constant substrate. We suggest that the visibility of the Ptolemy project can be increased by finding the substrate with a higher dielectric constant or increasing the height of the helium ion. Moreover, from the X-ray edge, metallic foil is not a good choice compared to graphene.

Contents

Version of July 12, 2021– Created July 12, 2021 - 12:37

Chapter 1

X ray singularity problem

1.1 Introduction

The well-known cosmic microwave background (CMB) is discovered by Penzias and Wilson [1], and it supported the Big Bang model. From the data of WMAP (Wilkinson Microwave Anisotropy Probe), 2001 [2] and Planck in 2013 [3], it is found that the age of the universe is about 13 billion years. However, it is tough to probe the universe closer than 300 000 years to the Big Bang from CMB since photons start decoupling at a temperature of about 3000 K. Therefore, Astronomers tend to seek another messenger that has a weaker interaction with matter than photons do.
Neutrinos have such a weak interaction with matter that they decouple from the matter 1 second after the Big Bang, making neutrino a perfect candidate to help people understand what happens in the very early universe. However, every coin has two sides; it is hard to detect the Cosmic Neutrino Background ($C\nu B$) directly because of its weak interaction with matters and its low energy. Nevertheless, many proposals have been formed based on the tritium beta decay [4, 5].
Beta-decay is a type of radioactive decay in which an atomic nucleus emits a beta particle [6]. In this process, either a neutrino is absorbed, or an antineutrino is released.

$$\nu_e + {}^3\mathrm{H} \rightarrow {}^3\mathrm{He} + e^-, \tag{1.1}$$

or

$${}^3\mathrm{H} \rightarrow {}^3\mathrm{He} + e^- + \bar{\nu}_e \tag{1.2}$$

As depicted in Fig. 1.1, the spectrum consists of the beta decay background part and the CNB part. The smoking gun signature of a relic neutrino capture is a peak in the spectrum, shifted about $2m_\nu$ above the beta decay end-

Version of July 12, 2021– Created July 12, 2021 - 12:37

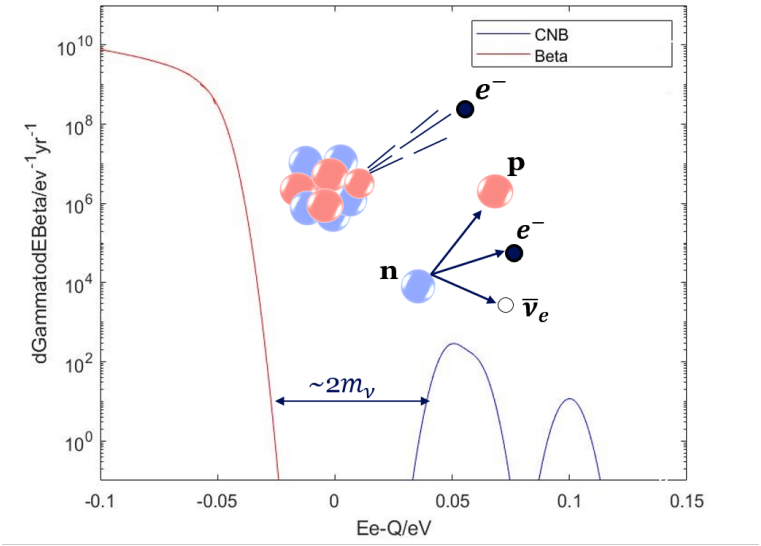

Figure 1.1: *Beta decay spectrum and the sketch of the beta decay process*

point. The two narrow peaks in the spectrum come from the contributions of different mass eigenstates. The energy gap is only about 100 meV, so the CNB signal can only be directly probed if the energy resolution of the experiments has the same order of magnitude of the neutrino mass. However, even for nowadays most advanced CNB detector Katrin, it can only achieve an energy resolution up to 0.93 eV [5]. Several effects can cause the spectrum broadening, which decreases the energy resolution significantly. For gaseous tritium, the most important one is the energy uncertainty due to the zero-point motion of molecules, which causes a broadening of the spectrum, leading to an insufficient energy resolution [5, 7].

Besides the requirement of high energy resolution, sufficient number density is another requirement to detect the CNB signal directly. The capture of the relic neutrino is so rare that if one wants to see about four events per year, then one needs to ensure that the effective mass of tritium atoms is at least 100g [8, 9]. However, the inelastic scattering between the electron and tritium set a constraint on the effective mass of tritium since only the electrons escape the source within the mean free path contribute to the signal; otherwise, they only yield the background [10, 11]. In the following discussion, we will show that due to this constriction, to contain a sufficient amount of tritium, one needs to build a huge setup, which is not feasible in engineering.

For a cylindrical container like the one in the Katrin project, the effective

mass of tritium molecules depends on the product of number density of tritium ρ and the mean free path of electrons l,

$$m_{eff} = m\rho lS, \tag{1.3}$$

where m is the mass of a single tritium atom, and S is the cross-sectional area of the tritium container. Hence, improving the tritium source strength can increase the tritium's effective mass. Nevertheless, increasing the number density of tritium decreases the mean free path of electrons as well.

$$l = (\rho\sigma_{e-T})^{-1}, \tag{1.4}$$

σ_{e-T} is the scattering cross-section for the inelastic scattering between electrons and tritium molecules, and $\sigma_{e-T} \sim 10^{-18}cm^2$ [5]. Combining those two equations, we can find that the effective mass of tritium molecules is a constant if the cross-section area of the container is fixed.

$$m_{eff} = mS\sigma_{e-T}^{-1} \tag{1.5}$$

Also, we can find the length scale to contain tritium with an effective mass of 100 grams,

$$l = S^{1/2} = \sqrt{N_{eff}\sigma_{e-T}}, \tag{1.6}$$

where N_{eff} is the number of molecules in 100 grams of tritium molecule. Therefore, the minimum area of the container should be $1000m^2$, which seems to be infeasible technically. For the actual setup of Katrin, the cross-section area of the container is about $50cm^2$, so the effective mass of tritium molecules is only about $50\mu g$ [5] even if one can provide a tremendous amount of tritium molecules.
Generally, for a spherical container, the minimum volume to contain tritium molecules is also too large to achieve in engineering. In the following discussion, we show that the length scale of a spherical container is the same as the cylindrical one. If the size of the container L is larger than the mean free path of tritium, then the effective mass of tritium should be

$$m_{eff} = m\rho l^3. \tag{1.7}$$

Inserting eq. (1.4) into the above expression, it gives the same result as in the eq. (1.6) Now, we can do an estimation about the minimum volume to contain 100g tritium. If we want to ensure that the effective mass of tritium is 100g, the container's volume should satisfy that

$$V = N/\rho = N\sigma_{e-t}\sqrt{N_{eff}\sigma_{e_T}} \geq (N_{eff}\sigma_{e-T})^{3/2}, \tag{1.8}$$

N is the total number of tritium molecules in the containers. If the container's size is smaller than the mean free path, we can get the following inequality.

$$N_{eff} = \rho V \leq \rho l^3 = l^2 \sigma_{e-T}^{-1} \tag{1.9}$$

Therefore, the volume of the tritium source must meet the following condition.

$$V = N_{eff}/\rho = N_{eff} l \sigma_{e-T} \geq (N_{eff}\sigma_{e-T})^{3/2} \tag{1.10}$$

In conclusion, the minimum volume to contain 100 grams of tritium molecules should be $(N_{eff}\sigma_{e-T})^{3/2} \sim 10^5 m^3$, which is a substantial technical challenge to achieve. One may argue that we can condense the tritium gas into a liquid state or even a solid-state to increase the number density and decrease the size of the setup. However, it encounters the problem that the molecule vibration in a solid-state or liquid state is even more robust, leading to an even lower energy resolution, so one cannot condense the tritium gas. To get rid of the molecular vibration and to increase the number of tritium per volume, as well as to provide a very high energy resolution, a setup is proposed by Ptolemy Collaboration [12, 13].
In the Ptolemy proposal, tritium atoms are localized by graphene sheet, which can be done by chemisorption or physisorption. The binding energy in both cases is smaller than the molecular binding energy, so the energy uncertainty due to the zero-point motion of the molecules can be reduced. To suppress the background, it uses radio-pure materials. Moreover, the ejected electrons are accelerated by the gate voltage, and they follow a vacuum trajectory until they exit the layer or bounce into another Field Effective Transistors(FET). Hence, they follow a FET-FET trajectory as depicted in Fig. 1.2. The hopping between different FETs is elastic, so electrons do not lose any energy during this process. Therefore, the Ptolemy project provides a very high energy resolution. Because so many graphene sheets can be stacked together, it provides a large enough density of tritium atoms. We can have a quantitative estimation of the size of the Ptolemy setup. For a fully tritiated graphene, the tritium atom density is about $3 \times 10^{15}/cm^2$ [9, 14], so the total effective area for 100 grams of tritium atoms is about $10^{10} cm^2$. The vertical separation of different graphene sheets is $\sim mm$ in z direction [15], so the entire setup can fit inside a $\sim 10^3 m^3$ space, which is two orders of magnitude smaller than the minimum volume in three dimensions. Furthermore, one can even find a non-planar topology to decrease the total volume of the setup by a factor of 100 [9]. However, there are still some emergent phenomena that are significant to the experiments. One of the phenomena that I am interested in

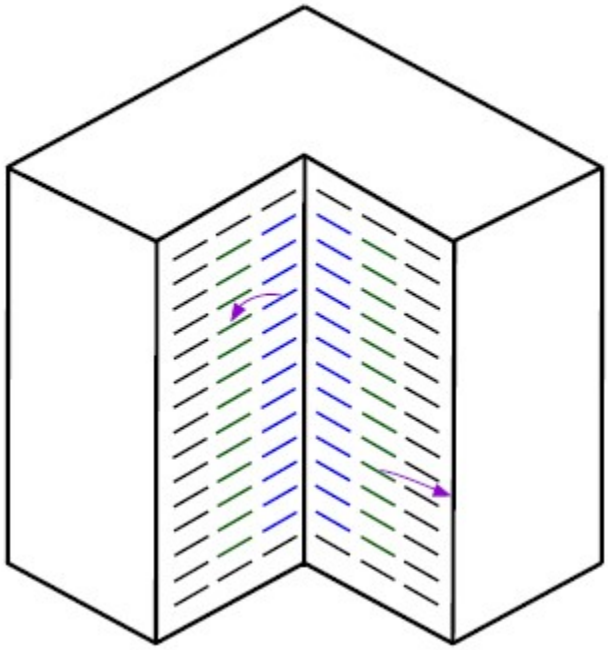

Figure 1.2: *Stacked planar arrays of graphene FET. [12]. Graphene Field Effect Transistors (G-FETs) are stacked together to construct an array. When an electron is emitted from a G-FET, it is deflected by the electrical field, and the electron follows the FET-FET trajectory.*

is the X-ray singularity effect [16], which is an instantaneous effect.

1.2 Defining the problem

In this section, we will define the problem and go into its details. This section is structured as follows, firstly, the physical description of the problem; second, the assumptions; then, it follows the calculation details. Assume that a tritium atom is placed right above a graphene sheet, and the graphene confines it by Van der Waals force or chemical binding. After capturing an incoming neutrino, the tritium atom converts into a helium ion, releasing an outgoing electron at the same time due to the induced β decay as depicted in Fig(1.3). The helium ion is positively charged, so it will become a scattering center in the graphene system and thus affects the graphene's electronic structure. Therefore, the system will respond to

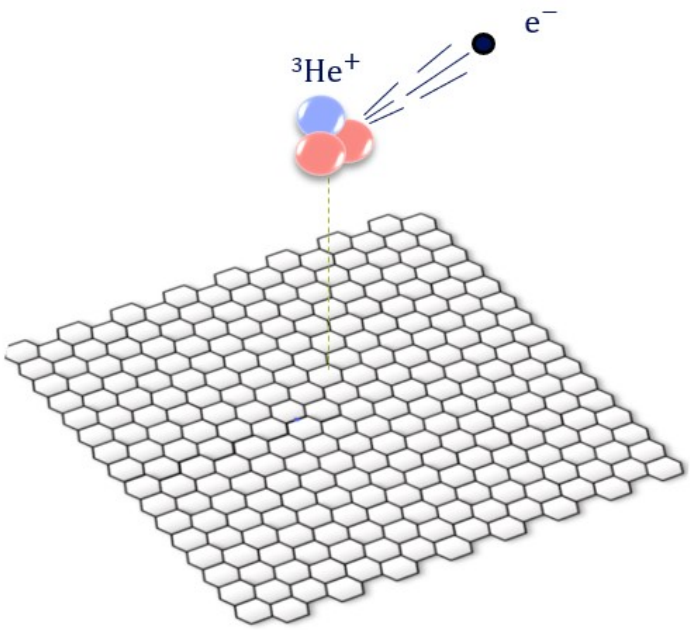

Figure 1.3: *Sketch of the beta emitter and graphene sheet.* $^3He^+$ *is the production of tritium beta decay, and it introduces a sudden localized perturbation in the electron system of graphene. This sudden localized perturbation causes an X-ray edge, which changes the beta decay spectrum.*

the sudden perturbation of the helium ion, which is the same as the X-ray singularity problem. In the X-ray singularity problem, the x-ray absorption creates a core level hole, and it becomes a scattering center, leading to Anderson Orthogonality Catastrophe (AOC) [17]. The AOC effect causes a singularity behavior in the absorption and emission spectrum. In our case, helium ion is like the core hole in the X-ray singularity problem. Due to Heisenberg's uncertainty principle, an energy transfer between the beta emitters and the graphene system can occur in a very short time. Without the interaction between the helium ion and graphene electrons, the response to this energy uncertainty is a delta function. However, the sudden perturbation of the helium ion changes this energy response from the delta function to a power-law decay function with an X-ray edge. Therefore, the emission spectrum of the β decay will be changed by this X-ray edge.

To simplify this problem, we can make the following assumption:
(1) The recoil effect between the outgoing electron and the helium ion on the X-ray singularity can be neglected. The recoil of the helium ion is about 3.38 eV, which has the same magnitude of order as the Fermi energy. The

mass of the helium ion is about 6000 times bigger than the mass of an electron, so we are safe to say the helium ion is localized. Also, whether for physisorption or chemisorption, the helium ion is confined in a potential well near the surface. Therefore, we can regard the helium ion as localized.
(2) We neglect the electron interaction in the graphene sheet, but we include the electron interaction effect in the self-consistent Hamiltonian of graphene instead.
(3) We assume there are no internal structures that are significant for our problem in the helium ion. The helium ion can occupy different excited states other than the ground state, but the lifetime of the excited state is estimated as $\hbar/\Delta E \approx 1.6 \times 10^{-17} s$, where$\Delta E$ is the energy level, $40.813 eV$ [18]. The mean free time of pure graphene is about one ps, and it is about 10 fs in metals. The lifetime is much less than the mean free time of electrons in the materials so that we can regard the helium ion as structureless.
(4) We assume the electrons in the graphene are isotropic before and after the transition.
(5) We assume the position of the helium ion relative to the graphene sheet is insignificant.
(6) We assume the helium ion is screened instantaneously.
(7) We assume the lifetime of helium ions is infinitely long. As long as the lifetime of helium ion is longer than the resolution time, our assumption is valid.
(8) We assume the kinetic energy of the outgoing electron takes the non-relativistic form. The assumption is valid since the kinetic energy of the incoming neutrino is about 18.6 KeV, which is one order of magnitude smaller than the rest mass of energy of an electron.
(9) In the physisorption case, the tritium only has Van der Waals interaction with the graphene sheet before the transition, and it is insignificant to our problem. The Van der Waals energy is about 100 meV [19, 20], but the electrostatic energy between helium ion is about 1 eV. Therefore, we can ignore the interaction between the tritium atom and the graphene sheet. Thus, the argument validates the assumption.
From the assumptions, it follows that the Hamiltonian takes the form as:

$$H = H_0 + H_I + H_{h-g} \tag{1.11}$$

which comprises the kinetic part, interaction part and the coupling between the helium ion and graphene. The kinetic part is trivial, and it is the

summation of the kinetic energy of each particle.

$$\begin{aligned} H_0 =& m_\nu c^2 \int \nu^\dagger \nu d^3x + m_h c^2 \int h^\dagger h d^3x + m_t c^2 \int t^\dagger t d^3x + \sum_k e_k^\dagger e_k \left(\frac{\hbar^2 k^2}{2m_e} + m_e c^2 \right) \\ &+ \sum_s \int d^2x \psi_s^\dagger(x)(-i\hbar v_F \vec{\nabla} \cdot \vec{\sigma}) \psi_s(x) \end{aligned} \tag{1.12}$$

m_ν is the mass of a neutrino, m_h is the mass of helium ion, and m_t is the mass of the tritium atom. The ionization energy of the helium atom is insignificant compared to the emission energy of beta decay so that we can ignore the energy difference between the helium ion and helium atom. $\nu^\dagger$ is the creation operator for the neutrino, $h^\dagger$ is the creation operator for helium ion, $t^\dagger$ is the creation operator for the tritium ion, $e_k^\dagger$ is the creation for the outgoing electron, v_F is the Fermi velocity, and s denotes the sublattice pseudospin sets, $\psi_s^\dagger(r)$ and $\psi_s(r)$ are the filed operators for the electrons in the graphene.

$$H_I = \int G_F \nu t h^\dagger e^\dagger d^3x \tag{1.13}$$

where G_F is the Fermi coupling constant [6, 21].
Because the potential well near the graphene surface extremely localizes the helium ion, only the ground state is significant for our purpose. Thus, the density operator of helium ion can be written as $h^\dagger(x)h(x) = h_0^\dagger h_0 \delta(x)$. We can construct the coupling Hamiltonian between the Helium ion and the electrons in the graphene as follow:

$$\begin{aligned} H_{h-g} &= -\int\int \rho(x) V(x-y) h^\dagger(y) h(y) d^2x d^3y \\ &= -\int \rho(x) \int V(x-y)\delta(y) h_0^\dagger h_0 d^3y d^2x \\ &= -\int \rho(x) V(x) h_0^\dagger h_0 d^2x \end{aligned} \tag{1.14}$$

$$V(x) = \frac{e^2}{4\pi\epsilon\epsilon_0\sqrt{d^2+x^2}} \tag{1.15}$$

where ϵ is the dielectric constant of the graphene, and ϵ_0 is the permittivity of vacuum. Under random phase approximation, we can obtain the effective dielectric constant of graphene.

$$\begin{aligned} \epsilon &= \frac{1+\kappa}{2} + \frac{2\pi e^2}{q} \frac{g_s g_v q}{16\hbar v_F} \\ &= \frac{1+\kappa}{2} + \frac{\pi e^2}{2\hbar v_F} \end{aligned} \tag{1.16}$$

where κ is the external dielectric constant of the substrate, the degeneracy factor $g_s = 2, g_v = 2$, and $v_F \approx 10^6 m/s$. If the graphene is suspended in vacuum, then $\epsilon \approx 4.4$. The height d denotes the distance between the helium ion and the graphene, and $\rho(x) =: \psi^\dagger(x)\psi(x)$: denotes the number density of electrons in the graphene. Using Fermi's golden rule, we can immediately get the transition probability.

$$W = \frac{2\pi}{\hbar} \sum_f \left| \langle 0|_t \langle 0|_\nu \langle k|_e \langle 1|_h \langle \lambda| \int G_F \nu d h^\dagger e^\dagger d^3x |1\rangle_t |1\rangle_\nu |0\rangle_e |0\rangle_h |FS\rangle \right|^2 \times \delta(E_f - E_i) \tag{1.17}$$

where $|\lambda\rangle$ is the final state of the graphene with the energy E_λ and $|FS\rangle$ is the Fermi sea of the graphene with energy E_0. The total energy of final state in the process is $m_e c^2 + \frac{\hbar^2 k^2}{2m_e} + E_\lambda + m_h c^2$, and the energy of initial state is $m_v c^2 + m_t c^2 + E_0$. The final state is the tensor product of the neutrino state, the outgoing electron state, and the graphene electron state. We can sum over the normal beta decay part and graphene part independently. We use index f' to denote the final state of beta decay and use index λ to denote the final state of electrons in graphene. Moreover, we can express the total transition probability as a convolution of the transition probability function of beta decay and graphene spectral density function. Hence, the expression of the total transition probability can be simplified to

$$\begin{aligned} W &= \frac{2\pi}{\hbar} \sum_{f'} \sum_\lambda |V_{if'}|^2 |\langle \lambda | FS \rangle|^2 \int \delta(E + E_\lambda - E_0) \delta(E_k - Q - E) dE \\ &= \frac{2\pi}{\hbar} \int \sum_{f'} \sum_\lambda |V_{if}|^2 |\langle \lambda | FS \rangle|^2 \delta(E + E_\lambda - E_0) \delta(E_k - Q - E) dE \\ &= (\Gamma * A)(E_k). \end{aligned} \tag{1.18}$$

$Q = m_t c^2 + m_v c^2 - m_e c^2 - m_h c^2$, and it is the emission energy of tritium beta decay, specifically, Q=18. 6KeV. $\Gamma(E)$ is the conventional beta decay transition rate, and $A(E)$ is the graphene spectral density function. Following the convention, we can regard $\frac{dW}{dE_k}$ as smeared beta decay rate at given electron kinetic energy.

$$\frac{d\Gamma}{dE_{k\,smeared}} = \frac{dW}{dE_k} = \int \frac{d\Gamma}{dE_k}(E_k - E) A(E) dE = (\frac{d\Gamma}{dE_k} * A)(E_k) \tag{1.19}$$

The discussion above also valid for the process of background neutron decay. We have found out that the smeared beta decay spectrum is nothing but the convolution between the spectral density function of graphene and the original beta decay spectrum. This result is vital to us since it tells us the influence of the X-ray edge in the Ptolemy project. Later, we will show that the spectral density function does have an X-ray edge.

1.3 Linked Cluster Expansion

The spectral density function A(E) is a quantity of physical interest, so we will investigate its property further in this section. The expression for it is

$$\begin{aligned} A(E) &= \sum_{\lambda} |\langle \lambda | FS \rangle|^2 \, \delta(E + E_\lambda - E_0) \\ &= \frac{1}{2\pi\hbar} \sum_{\lambda} \int dt \, \langle FS | \, e^{-iH_\lambda t} \, | \lambda \rangle \, \langle \lambda | FS \rangle \, e^{-i(E-E_0)t/\hbar} \\ &= \frac{1}{2\pi\hbar} \int dt < FS | e^{-iH_\lambda t/\hbar} | FS > e^{iE_0 t/\hbar} e^{-iEt/\hbar}, \end{aligned} \tag{1.20}$$

where H_λ is the Hamiltonian of the graphene after the beta decay. We can express it in momentum space,

$$H_\lambda \sum_s \sum_k s\hbar v_F k C^\dagger_{ks} C_{k's} - \frac{1}{L^2} \sum_{ss'} \sum_{kk'} V(k,k') F_{ss'}(k,k') C^\dagger_{ks} C_{k's} h^\dagger_0 h_0 \tag{1.21}$$

with

$$F_{ss'}(k,k') = \frac{1}{2} \left[ss' + \exp(i\theta_k - i\theta_{k'}) \right] \tag{1.22}$$

and

$$V(k,k') = \frac{2\pi e^2 \exp\left(-|k'-k|d\right)}{\epsilon |k-k'|} \tag{1.23}$$

where s is the index for the band index. To simplify this problem, we can omit the exponential factor in the potential, and then it becomes

$$V(k,k') = \frac{2\pi e^2}{\epsilon |k-k'|} \tag{1.24}$$

Although this crude simplification is only valid near the edge of the spectral density function, it gives us a physics insight in the first step. Later, we will recover the effect of the distance d in the next chapter. For the detailed

Version of July 12, 2021– Created July 12, 2021 - 12:37

calculation about the Hamiltonian and the discussion on this simplification, please see Appendix A1.
To calculate the spectral density function A(E), we can define a density function.

$$\rho(t) = \left\langle \mathrm{FS}|\mathrm{e}^{-iH_\lambda t/\hbar}|\mathrm{FS}\right\rangle \mathrm{e}^{iE_0 t/\hbar} \tag{1.25}$$

A(E) is just the Fourier transform of it.
We can recognize $-i\Theta(t)\rho(t)$ as the core hole Green function in the conventional X-ray singularity problem [16, 22–25]. The density function $\rho(t)$ can be expressed in another way.

$$\begin{aligned}\rho(t) &= \left\langle \mathrm{FS}|\mathrm{e}^{-iH_\lambda t/\hbar}\mathrm{e}^{iH_{FS}t/\hbar}|\mathrm{FS}\right\rangle \\ &= \left\langle \mathrm{T}\exp\left[-\mathrm{i}\int_0^{\mathrm{t}} \mathrm{V}(\mathrm{t}_1)\mathrm{dt}_1\right]\right\rangle\end{aligned} \tag{1.26}$$

H_{FS} is the unperturbed Hamiltonian of the graphene sheet, T is the time ordering operator, and V(t) is the interaction term. Using linked cluster expansion method [25–27], we can evaluate the expression above.

$$\left\langle T\exp\left[-i\int_0^t V(t_1)dt_1\right]\right\rangle = \exp\left[\sum_l F_l(t)\right] \tag{1.27}$$

where

$$F_l(t) = \frac{(-i)^l}{l}\int_0^t dt_1 \cdots \int_0^t dt_l \left\langle TV(t_1)\cdots V(t_l)\right\rangle_{connected} \tag{1.28}$$

The first term is just the self-energy term E_i, so it can be absorbed into the threshold energy. Assuming the interaction is weak, we can restrict ourselves to the second term [25].

$$F_2(t) = -\int_0^\infty \frac{du}{u^2} R_e(u)(1-\mathrm{e}^{-iut}) \tag{1.29}$$

where

$$Re(u) = \frac{1}{\pi L^2}\sum_q |V(q)|^2 \Lambda(q,u) \tag{1.30}$$

and

$$\Lambda(q,u) = \mathrm{Im}P^{(1)}(q,u). \tag{1.31}$$

where $P^{(1)}(q,u)$ is the polarizability function. We will prove it in the following steps. According to Wick's theorem, we can pair the operators in

Version of July 12, 2021– Created July 12, 2021 - 12:37

the expression of $F_2(t)$ to evaluate it.

$$\begin{aligned} F_2(t) &= \frac{g'}{2V^2}\int_0^t dt_1\int_0^t dt_2 \sum_{k_1,k_2}|V(k_1,k_2)|^2 G(k_2,t_1-t_2)G(k_1,t_2-t_1) \\ &= \frac{1}{2V}\int_0^t dt_1\int_0^t dt_2\sum_q |V(q)|^2\int_{-\infty}^{\infty} i\chi_e(q,u)e^{-iu(t_1-t_2)}\frac{du}{2\pi} \\ &= \frac{1}{2\pi V}\int_0^\infty \sum_q |V(q)|^2 i\left[\chi_e(q,u)-\chi^*(q,u)\right]\frac{1-e^{-iut}}{u^2}du \\ &= -\frac{1}{\pi V}\int_0^\infty \sum_q |V(q)|^2 \mathrm{Im}\chi_e(q,u)\frac{1-e^{-iut}}{u^2}du \end{aligned} \tag{1.32}$$

and

$$\begin{aligned} \chi_e(q,u) &= \frac{-ig'}{V}\sum_p\int_{-\infty}^{\infty}|F_{ss'}(p,p+q)|^2 G(p+q,t)G(p,-t)e^{iut}dt \\ &= \frac{-ig'}{L^2}\int_{-\infty}^{\infty}\frac{dE}{2\pi}\sum_{p,s,s'}|F_{ss'}(p,p+q)|^2 G_{s's'}(p+q,E+u)G_{ss}(p,E), \end{aligned} \tag{1.33}$$

where $G_{ss}(P,E)$ is the Green function for graphene, and $g' = g_s g_v$. In the third step of eq. (1.32), we have used the property of $\chi_e(q,-u) = \chi_e^*(q,u)$. In the clean limit, $\chi_e(q,u) = P^{(1)}(q,u)$ [25, 28]. we just quote the result in the references [29–31] and its calculation details can be found in the Appendix A2. From eq. (5.13), one can obtain that

$$\Lambda(q,u) = \frac{q^2}{4\sqrt{u^2-v_F^2q^2}}\Theta(u-v_Fq) \tag{1.34}$$

Substituting it into eq. (1.30), then we have

$$R_e(u) = e^4\int_0^{u/v_F}\frac{qdq}{2\epsilon^2\sqrt{u^2-v_F^2q^2}} = \frac{e^4u}{2\epsilon^2v_F^2} = gu \tag{1.35}$$

Using the effective dielectric constant we get in the previous step, we can find $g \approx 0.125$. Substituting it into the expression of F_2, thus one can get

$$F_2(t) = -g\int_0^{\xi_0}\frac{(1-e^{-iut})du}{u} \approx -g\int_{1/it}^{\xi_0}\frac{du}{u} \approx -g\ln(1+it\xi_0) \tag{1.36}$$

The expression in valid only for large t, i. e $\xi_0 t >> 1$. The expression for the density function is obtained from eq. (1.36),

$$\rho(t) = \exp(-iE_i t - g\ln(1 + it\xi_0)). \tag{1.37}$$

1.4 Result

In this section, we found out that the spectral density function of graphene, which is the gamma distribution function. The Fourier transform of eq. (1.37) gives the spectral density function of graphene at the given energy.

$$\begin{aligned} A(\Omega) &= \int_{-\infty}^{\infty} \frac{dt}{2\pi} e^{-iEt}\rho(t) \\ &= \int_{-\infty}^{\infty} \frac{dt}{2\pi} \frac{e^{-it\Omega\xi_0}}{(1+it\xi_0)^g} \\ &= \Theta(-\Omega)\frac{\sin(\pi g)}{\pi}\Gamma(1-g)\frac{\exp(\Omega)}{\xi_0(-\Omega)^{(1-g)}} \end{aligned} \tag{1.38}$$

with

$$\Omega = (E + E_i)/\xi_0 \tag{1.39}$$

The spectral density function strictly obeys the gamma distribution, and the result coincides with that for a metal with a local constant interaction [25–27]. The gamma distribution function has two parameters: one is the shape parameter, which is the coupling constant in our problem, and another one is the scale parameter, which is the cut-off energy in our case, but now it remains unknown. We plot it by using Mathematica. As we can see in Fig. 1.4, the function is divergent when Ω goes to zero. It means there is no energy transfer between the outgoing electron and the graphene sheet, so the state of graphene is unperturbed. Hence, the overlap between the two identical Slater determinants gives a delta function, leading to the divergent behavior in the vicinity of $\Omega = 0$.

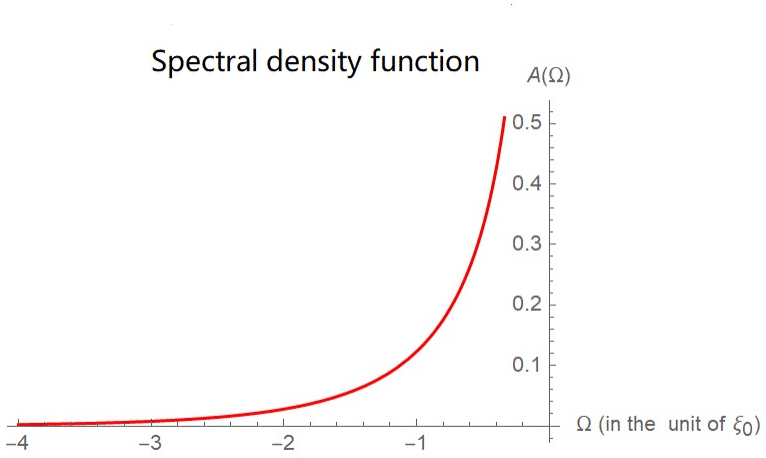

Figure 1.4: *The spectral density function of graphene at a given energy.* $A(\Omega)$ *describes the possibility of graphene absorbing the outgoing electron's energy. The energy is measured in the unit of cut-off energy* ξ_0.

Chapter 2

Further Study

2.1 Influence of Height

In the previous discussion, we have got the spectral density function and find its shape parameter, i.e., the coupling constant, but the cutoff energy is still unknown. This section shows that natural cutoff energy can be found if we consider the effect of the height of helium ions from the graphene sheet. In this case, the expression of $Re(u)$ should be

$$R_e(u) = e^4 \int_0^{u/v_F} \frac{qe^{-2qd}dq}{2\epsilon^2\sqrt{u^2 - v_F^2 q^2}} = gu + \frac{\pi g u}{2}[L_1(\frac{2du}{v_F}) - I_1(\frac{2du}{v_F})] \quad (2.1)$$

where $L_1(\frac{2du}{v_F})$ and $I_1(\frac{2du}{v_F})$ are modified Struve function and modified Bessel function, respectively.
Substituting $Re(u)$ into the term $F_2(t)$, one can find that

$$F_2(t) = -g\int_0^{\xi_0} \frac{(1-e^{-iut})du}{u} - \frac{\pi g}{2}\int_0^{\xi_0}[L_1(\frac{2du}{v_F}) - I_1(\frac{2du}{v_F})]\frac{(1-e^{-iut})du}{u} \quad (2.2)$$

The first integration is the original term, labeled as $F_2^0(t)$ and the second integration is the correction term, labeled as $F_2'(t)$. Directly evaluating the

correction term is difficult, but we can express it as a double integral.

$$\begin{aligned} F_2'(t) &= g\int_0^{2d\xi_0/v_F}\int_0^1 e^{-zx}\sqrt{1-x^2}(1-e^{-izv_Ft/2d})dxdz \\ &= g\int_0^1 \sqrt{1-x^2}\left(\frac{1-e^{-2dx\xi_0/v_F}}{x}\right)dx + g\int_0^1 \sqrt{1-x^2} \\ &\times \left(\frac{-1+\exp(-it\xi_0-2dx\xi_0/v_F)}{x+iv_Ft/2d}\right)dx \\ &= P(\xi_0)+N(\xi_0,t) \end{aligned} \tag{2.3}$$

where z=$2du/v_F$. From the calculation above, we can find that the correction term can be split into two terms. The first part is a constant independent of time t, and the second part is a time-dependent function. Hence, only the function $N(\xi_0,t)$ is significant to our calculation. Obviously, if t=0, it cancels with the first term $P(\xi_0)$. However, when t approaches infinity, the correction term $F_2'(t)$ should equal to $P(\xi_0)$.
We need to make some approximations to evaluate the function $N(\xi_0,t)$. At a large time limit, roughly, we can use 1 to replace the ugly square root $\sqrt{1-x^2}$ since most contributions to the integration in $P(\xi_0)$ and $N(\xi_0,t)$ come from the vicinity of x=0. Then, we can write the correction term $F_2'(t)$ in a simple way.

$$\begin{aligned} F_2'(t) &= g\int_0^1\left(\frac{1-e^{-2dx\xi_0/v_F}}{x}\right)dx + g\int_0^1\left(\frac{-1+\exp(-it\xi_0-2dx\xi_0/v_F)}{x+iv_Ft/2d}\right)dx \\ &= g\int_0^1\left(\frac{1-e^{-2dx\xi_0/v_F}}{x}\right)dx - g\int_{iv_Ft/2d}^{1+iv_Ft/2d}\left(\frac{1-\exp(-2dy\xi_0/v_F)}{y}\right)dy \\ &= g\int_0^1\left(\frac{1-e^{-2dx\xi_0/v_F}}{x}\right)dx + g\int_0^{iv_Ft/2d}\left(\frac{1-\exp(-2dy\xi_0/v_F)}{y}\right)dy \\ &- g\int_0^{1+iv_Ft/2d}\left(\frac{1-\exp(-2dy\xi_0/v_F)}{y}\right)dy \end{aligned} \tag{2.4}$$

The factor $1-\exp(-2dy\xi_0/v_F)$ behaves as $2dy\xi_0/v_F$ in the limit where $u\to 0$. We can use $\frac{v_F}{2d\xi_0}$ to replace the lower limit of the integration, since $\frac{v_F}{2d\xi_0} \ll 1$. At very large time t, we can omit the factor $\exp(-2dy\xi_0/v_F)$. Hence, the correction term $F_2'(t)$ can be approximately expressed as a very

Version of July 12, 2021– Created July 12, 2021 - 12:37

neat form.

$$\begin{aligned} F_2'(t) &\approx g\int_{v_F/(2d\xi_0)}^{1}\frac{dx}{x}+g\int_{v_F/(2d\xi_0)}^{iv_Ft/2d}\frac{dy}{y}-g\int_{v_F/(2d\xi_0)}^{1+iv_Ft/2d}\frac{dy}{y} \\ &\approx g\ln(1+\frac{2d\xi_0}{v_F})+g\ln(i\xi_0t+1)-g\ln(i\xi_0t+\frac{2d\xi_0}{v_F}+1) \end{aligned} \tag{2.5}$$

Substituting this result into equation (2.2), and using equation (1.27) and equation (1.38), one can obtain the expression of spectral density function of graphene.

$$\begin{aligned} A(\Omega') &= \int_{-\infty}^{\infty}\frac{dt}{2\pi}e^{-iEt}\exp(F_2^0(t)+F_2'(t) \\ &= \int_{-\infty}^{\infty}\frac{dt}{2\pi}\frac{\exp\left(-it\Omega'\frac{\xi_0}{1+2d\xi_0/v_F}\right)}{(1+it\xi_0)^g}\frac{(1+2d\xi_0/v_F)^g\,(1+i\xi_0t)^g}{(1+2d\xi_0/v_F+i\xi_0t)^g} \\ &= \int_{-\infty}^{\infty}\frac{dz}{2\pi}\frac{1+2d\xi_0/v_F}{\xi_0}\frac{\exp\left(-i\Omega'z\right)}{(1+iz)^g} \\ &= \Theta(-\Omega')\frac{\sin(\pi g)}{\pi}\Gamma(1-g)\frac{\exp(\Omega')}{\xi'(-\Omega')^{(1-g)}} \\ &= \Theta(-\Omega')\frac{\exp(\Omega')}{\Gamma(g)\xi'(-\Omega')^{(1-g)}} \end{aligned} \tag{2.6}$$

where $\xi' = \frac{\xi_0}{1+2d\xi_0/v_F}$, and $\Omega' = (E+E_i)/\xi'$.
The cut-off energy ξ_0 is entirely arbitrary, but we can get a natural cut-off energy ξ when we extend ξ_0 to infinity.

$$\xi = \lim_{\xi_0\to\infty}\frac{\xi_0}{1+2d\xi_0/v_F} = \frac{v_F}{2d} \tag{2.7}$$

We get nearly the same result as the previous one, eq. (1.38), only with different cutoff energy ξ. This result can be explained quite straightforward. From eq. (2.1), one can see that the Yukawa type potential recovers to a normal Coulomb potential if $q << 1/(2d)$, so the natural cutoff energy is $\xi = \hbar\frac{v_F}{2d}$. Now, we have found the scale parameter of the gamma distribution. From the eq. (2.7), one can see that the cutoff energy depends on the height d, so one can manipulate the cutoff energy by adjusting the height of the helium ion.

2.2 Results for metal

As suggested in reference [32], the zero-point motion of the tritium atom due to the chemical bonding causes the Ptolemy project to have very in-

Version of July 12, 2021– Created July 12, 2021 - 12:37

significant visibility. One way to fix this problem is to find a target material with substantially weaker lateral potential than graphene, so simple metal such as gold foil may be a good candidate. If we consider gold foil rather than graphene, the calculation is very similar. Assuming the area of the gold foil is very large, say $1m^2$, and the thickness of it is about 1 micrometer, we can regard the gold foil as a bulk material. Equation (1.19) still holds, but with a different spectral function. To calculate the spectral function of gold foil, we need to construct the effective Hamiltonian first.

$$H_G = \sum_{k\sigma} \frac{\hbar^2 k^2}{2m} C^\dagger_{k\sigma} C_{k\sigma} - \frac{1}{V} \sum_{k,q} \frac{V(q)}{\epsilon(q)} C^\dagger_{k+q,\sigma} C_k, \sigma \tag{2.8}$$

where $V(q)$ is the unscreened Coulomb potential, and it has the following form in three dimension.

$$V(q) = \frac{4\pi e^2}{q^2} \tag{2.9}$$

$\epsilon(q)$ is the static dielectric function. Under RPA [25, 33], it takes the form as

$$\epsilon(q) = 1 + \frac{q_{TF}^2}{2q^2} \left[1 + \frac{1}{2x}(1-x^2) \ln \left(\frac{1+x}{1-x} \right) \right]. \tag{2.10}$$

q_{TF} is the Thomas-Fermi wave vector, and $x = \frac{q}{2k_F}$. The equations (1.29) and (1.33) still hold but with a different polarization operator [25, 33].

$$\Lambda'(q,u) = u \left(\frac{m^2}{2\pi q} \right) \Theta(2k_F - q) \tag{2.11}$$

Substituting it into equation (1.30), one can obtain

$$R_e(u) = \begin{cases} gu & u < \xi_0 \\ 0 & u > \xi_0 \end{cases} \tag{2.12}$$

$$g = \frac{m^2}{2\pi^2} \int \frac{d^3q}{(2\pi)^3} \frac{V^2(q)}{\epsilon^2(q) q} \Theta(2k_F - q) \tag{2.13}$$

The upper limit of u is the cutoff energy x_0, which is determined by the range that the polarization operator is linear in u. The range is approximately $\xi_0 \sim E_F$. We can evaluate the coupling constant g numerically. Given at room temperature, the Fermi energy of gold is 5.51 eV, the Fermi wave vector of gold is $1.20 \times 10^{10} m^{-1}$, and the Thomas-Fermi wave vector of gold is $1.70 \times 10^{10} m^{-1}$ [34]. It thus follows that the coupling constant $g \approx 0.20$. The spectral density function is still the same as eq. (1.38), but

Version of July 12, 2021– Created July 12, 2021 - 12:37

with different cutoff energy and a different coupling constant.
If the thickness of the gold foil is thin enough, we can consider it as a two-dimensional material. In this case, the polarization operator is [33, 35, 36]

$$\Lambda(q,u) = \frac{m^2 u}{\pi k_F q \sqrt{1-\left(\frac{q}{2k_F}\right)^2}}\Theta(2k_F - q). \tag{2.14}$$

The Coulomb potential in the two dimension takes the form as

$$V(q) = \frac{2\pi e^2}{q}, \tag{2.15}$$

and the dielectric function $\epsilon(q)$ is obtained under RPA [33, 35, 36].

$$\epsilon(q) = 1 + \frac{2me^2}{q} \tag{2.16}$$

Therefore, repeating the same procedure in the three-dimensional case, one can obtain that

$$R_e(u) = \begin{cases} gu & u < \xi_0 \\ 0 & u > \xi_0 \end{cases} \tag{2.17}$$

$$g = \frac{m^2}{\pi^2 k_F}\int \frac{d^2q}{(2\pi)^2}\frac{4\pi^2 e^4}{q(q+2me^2)^2\sqrt{(1-\left(\frac{q}{2k_F}\right)^2}}\Theta(2k_F - q) \tag{2.18}$$

The upper limit ξ_0 is approximately equal to the Fermi energy E_F. The coupling constant is about 0.27.
In conclusion, whether in two dimensions or three dimensions, the spectral function of the simple metal is the same as the graphene's, but with a different coupling constant and different cutoff energy. For metal, the cutoff energy is entirely arbitrary and is not controllable compared to graphene. Additionally, the coupling constant is also fixed in metals, so we cannot tune it to increase visibility. In contrast, we can adjust the substrate's dielectric constant to make the coupling constant less than 0.1.

2.3 Influence of disorder

Until now, we only consider the intrinsic graphene, which is undoped and ungated. However, tritium atoms in graphene play the role of disorders,

which changes the mean free path and the density-density response function of electrons, so we need to take their effects seriously. If the resolution time is greater than the mean free time, i. e., $\tau_{res} >> \tau$, one needs to consider the diffusive effects, which change the polarizability function and thus the coupling constant. From eq. (1.20) and eq. (1.26), we learn that the only effect of the impurities on the spectral density function or density-density function is to drive the system into a different initial state rather than the Fermi sea. In the presence of many random impurities, we do not care about the effect of a specific impurity, so we only consider the impurity-average effect. The impurity-average density-density response function is [28, 33, 37]

$$\chi_0^{imp}(q,\omega) = \frac{\chi_0(q,\omega+\frac{i}{\tau})}{1+(1-i\omega\tau)^{-1}\left[\frac{\chi_0(q,\omega+\frac{i}{\tau})}{\chi_0(q,0)}-1\right]} \tag{2.19}$$

where τ is interpreted as momentum relaxation time or the quasiparticle lifetime. Apart from the electron-electron interactions, there are two scattering mechanisms in the normal metal. One is electron-phonon interaction, and the other is impurities or defects scattering. For simple metals with high electron density, the lifetime of quasiparticles near the Fermi level is infinitely large [38], so we do not need to consider the electron-electron interaction for a normal metal. The lifetime τ_0 due to the electron-phonon scattering can be obtained by measuring the conductivity of pure metal, and it is temperature-dependent. As for the impurity scattering, the expression of the lifetime τ_{imp} near the Fermi level take the form as [28, 33]

$$\frac{1}{\tau_{imp}} \equiv 2\pi n_{imp}|U(0)|^2 N(0) \tag{2.20}$$

$n_{imp} \sim 10^{25} m^{-3}$ represents the density of the impurities, N(0) is the density of state at Fermi level, and $U(0)$ is the external potential of the electrons at Fermi level. From eq. (2.20), one can obtain that the so-called momentum relaxation time or mean free time τ_{imp} is about $10^{-12}s$.
We can estimate the total momentum relaxation time using Matthiessen's rule.

$$\frac{1}{\tau} = \frac{1}{\tau_{imp}} + \frac{1}{\tau_0} \tag{2.21}$$

Under Room temperature, the mean free time τ_0 for pure gold is about 27.3 fs [34]. Hence, the magnitude order of the total mean free time is about 10^{-14} s at room temperature. The resolution energy $\hbar\omega_{res}$ is about

10 meV, and the resolution time satisfies $\tau_{res} = 1/\omega_{res} \sim 10^{-13}\ s$, so the energy window of 10 meV near the edge is most interesting for our problem. If $\omega_{res} \gg 1/\tau$, we can neglect the effect of impurities, and the density-density response function recovers to the Lindhard function. If $\omega_{res}\tau \ll 1$, we need to consider both diffusive and ballistic regimes, and the diffusive response function is

$$\chi^{imp}(q,\omega) = \frac{N(0)Dq^2}{Dq^2 + i\omega} \tag{2.22}$$

Then, $F_2(t)$ is given by [39]

$$F_2(t) = \frac{|\overline{U(0)}|^2}{\pi^2 g_0}\ln(1+it/\tau) + 2\overline{U(0)}|^2\left[1-\left(\frac{1}{k_F v_F \tau}\right)^2\right]\ln(1+i\xi t) \tag{2.23}$$

$\overline{U(0)} = U(0)N(0)$, and $g_0 = 2N(0)D_d v_F \tau$.
For metals, we estimate $k_F v_F \tau \approx 10^2 \gg 1$ and $g_0 \approx 10^3 \gg 1$ when $\tau \approx 10^{-14}\ s$, so the first term in eq. (2.23) is negligible compared to the second term. The result of eq. (2.23) recovers to the previous result in the clean limit.
Moreover, we can reduce the diffusive effect by decreasing the temperature. The excited modes of phonons are frozen under very low temperature, and the electron-phonon interaction thus is negligible. In that case, only impurity scattering contributes to scattering, and the mean free time satisfies $\tau \sim 10^{-12}\ s \gg 1/\omega$, so that we can neglect the impurity effect.
For pure graphene, the momentum relaxation time is about one ps [40, 41], and it is one order greater than the resolution time so that we can treat the electrons of graphene ballistically in the resolution time. However, the physisorption or chemisorption of tritium atoms on the graphene changes the mean free time of electrons. Electrons in graphene are not so dense as them in metals, so that impurities may have significant effects on the transport properties of graphene. For physisorption, the binding energy of the tritium atom is about 0.2 eV, so the potential difference between the tritium atom and carbon sheet is about 0.2 eV [19, 20, 42]. Since the order of electron energy is about 1 eV, most electrons change their momentum slightly. Therefore, we do not need to consider the impurity effects in the physisorption case.
However, it is very tricky in the chemisorption case since the binding energy has the same order of magnitude of the electrons' energy [42, 43]. For pure graphene, the hybridization of its electronic orbital is sp^2, contributing a π electron. For tritiated graphene, the chemical bonding between a tritium atom and a carbon atom changes the hybridization from sp^2 to sp^3.

The π orbital is tightly bounded for the sp^3 hybridization, so the tritium atom effectively acts as a vacancy. Thus, we can use the midgap model to characterize the potential induced by the tritium atoms [19, 44, 45]. The potential is profiled as

$$U(r) = \begin{cases} \infty, & \text{if } 0 < r \leq R' \\ U_0, & \text{if } R' < r \leq R \\ 0, & \text{if } r > R. \end{cases} \tag{2.24}$$

The mean free time is defined from the following expression

$$\frac{\hbar}{\tau_k} = \frac{8n_i}{\pi\rho(E_k)} \sin^2 \delta(k), \tag{2.25}$$

where $\rho(E_k)$ is the density of state of E_k, which has the explicit form as

$$\rho(E_k) = \frac{2E_k}{\pi\hbar^2 v_F^2} \tag{2.26}$$

and $\delta(k)$ is the phase shift of electrons with momentum k. Using the method in the paper [45], we can obtain the phase shift at $k \approx 0$.

$$\delta(k) = -\frac{\pi}{2} \frac{1}{\ln(2kR')} \tag{2.27}$$

. We expand the sine function in eq. (2.25) for $kR' \ll 1$. Thus it gives the mean free time

$$\begin{aligned} \tau_k &= \frac{\hbar\rho(E_k)}{2\pi n_i} (\ln kR')^2 \\ &= \frac{k}{\pi^2 v_F n_i} (\ln kR')^2 \end{aligned} \tag{2.28}$$

This expression depends on the energy. While, this function has a minimal value at $kR' = \mathrm{e}^{-2}$. The minimum value is

$$\tau_{min} = \frac{4\mathrm{e}^{-2}}{\pi^2 v_F n_i R'} \tag{2.29}$$

If τ_{min} is much greater than the resolution time, we can neglect the impurity effect. It means that

$$\frac{4\mathrm{e}^{-2}}{\pi^2 v_F n_i R'} \gg 1/\omega \sim 10^{-13}\, s \tag{2.30}$$

R' is about 1 Å, so we find the condition for a maximum impurity concentration.

$$n_i \ll \frac{4e^{-2}\omega}{\pi^2 v_F R'} = 5 \times 10^{11}/\mathrm{cm}^2 \tag{2.31}$$

We can also use another method to estimate the mean free time by using the scattering cross-section.

$$\frac{1}{\tau} = n_i v_F \sigma_{sca}. \tag{2.32}$$

σ_{sca} is the scattering cross-section, which has the dimensionality of length. Some researchers reported that the scattering cross-section for hydrogenated graphene is about 5 Å [46]. Then, the maximum impurity concentration is about $2 \times 10^{12}/\mathrm{cm}^2$, which has the same order of magnitude as the previous result. In conclusion, the safe concentration range is less than $5 \times 10^{11}/\mathrm{cm}^2$.

2.4 Dynamic Screening

The instantaneous screening assumption is not valid in the tail of the spectral function of graphene. While, if the weight of the tail is too high, it will cause the beta decay spectrum to broaden widely, and it may take many years to observe a single event. To get a more rigorous result, we need to consider the dynamic screening effect. The dynamic screening potential is

$$V(q,\omega) = \frac{V_i(q,\omega)}{\epsilon(q,\omega)} \tag{2.33}$$

For a sudden external potential [47],

$$V_i(q,\omega) = \frac{V(q)i}{\omega + i\delta}. \tag{2.34}$$

δ is an infinitesimal quantity, and $V(q) = \frac{2\pi e^2}{\kappa q}$ is the bare Coulomb potential. One can recognize that $\frac{1}{\epsilon(q,\omega)} - 1$ is the susceptibility function so that we can use the Kramers-Kronig relations.

$$\frac{1}{\epsilon(q,\omega)} - 1 = -\frac{1}{\pi}\int_{-\infty}^{\infty} d\omega' \mathrm{Im}\left(\frac{1}{\epsilon(q,\omega')} - 1\right)\frac{1}{\omega - \omega' + i\delta} \tag{2.35}$$

Substituting it into the expression of dynamic screening potential and performing the Fourier transform, one can find the time-dependent screening potential.

$$\begin{aligned} V(q,t) &= \int_{-\infty}^{\infty} V(q,\omega)\mathrm{e}^{-i\omega t}d\omega \\ &= V(q)\int_{-\infty}^{\infty} d\omega' \mathrm{Im}\left(\frac{1}{\epsilon(q,\omega')}-1\right)\left[\frac{i}{-\pi}\int_{-\infty}^{\infty} d\omega \frac{\mathrm{e}^{-\mathrm{i}!\mathrm{t}}}{(\omega+i\delta)(\omega-\omega'+i\delta)}\right] \\ &+ V(q)\theta(t) \\ &= \frac{V(q)\theta(t)}{\pi}\int_{-\infty}^{\infty}\frac{1-\mathrm{e}^{-\mathrm{i}!'\mathrm{t}}}{\omega'}\mathrm{Im}\left(\frac{1}{\epsilon(q,\omega')}-1\right)d\omega' + V(q)\theta(t) \end{aligned} \tag{2.36}$$

In the large time limit, the oscillating term disappears, so the potential becomes

$$V(q,\infty) = \frac{V(q)}{\epsilon(q,0)} \tag{2.37}$$

For graphene, $\epsilon(q,0)$ does not depend on q, so that we can denote $\epsilon(q,0)$ as ϵ. The first term in the last line vanishes in the short time limit, so the potential turns into the bare potential.

$$V(q,0) = V(q) \tag{2.38}$$

For an arbitrary time, we can express $V(q,t)$ as

$$V(q,t) = \frac{V(q)\theta(t)}{\epsilon(q,0)} - \frac{V(q)\theta(t)}{\pi}\int_{-\infty}^{\infty}\frac{\mathrm{e}^{-\mathrm{i}!'\mathrm{t}}}{\omega'}\mathrm{Im}\left(\frac{1}{\epsilon(q,\omega')}-1\right)d\omega' \tag{2.39}$$

For intrinsic graphene, the time-dependent potential is

$$\begin{aligned} V(q,t) &= \frac{V(q)\theta(t)}{\epsilon(q,0)} + V(q)\theta(t)T(v_F q t) \\ &= \frac{V(q)\theta(t)}{\epsilon(q,0)} - \frac{V(q)\theta(t)}{\pi}\int_{-\infty}^{\infty}\frac{\mathrm{e}^{-\mathrm{i}!\mathrm{t}}}{\omega}\frac{aq}{\sqrt{\frac{\omega^2}{v_F^2}-q^2}}\frac{\theta(|\omega|-v_F q)d\omega}{1+\left(\frac{aq}{\sqrt{\frac{\omega^2}{v_F^2}-q^2}}\right)^2} \\ &= \frac{V(q)\theta(t)}{\epsilon(q,0)} - \frac{2V(q)\theta(t)}{\pi}\int_1^{\infty}\frac{a\cos(\omega v_F q t)\sqrt{\omega^2-1}}{\omega\left(\omega^2-1+a^2\right)}d\omega, \end{aligned} \tag{2.40}$$

where $a = (\epsilon(q,0) - 1) = \frac{\pi e^2}{2\hbar\kappa v_F}$, and $T(v_F q t)$ is a one-variable fast-decay function that only depends $v_F q t$. When $t << 1, T(v_F q t) \approx \frac{1}{\epsilon(q,0)} - 1$, and when $t >> 1, T(v_F q t) \approx 0$
From the general expression of the $F_2(t)$, eq. (1.29), we can find that

$$\begin{aligned} F_2(t) &= \frac{1}{2}\int_0^t dt_1 \int_0^t dt_2 \int_0^\infty \mathrm{e}^{-\mathrm{iu}(\mathrm{t}_1-\mathrm{t}_2)} \frac{du}{\pi V} \sum_q V(q,t_1)V(q,t_2)\Lambda(q,u) \\ &= \frac{1}{2}\int_0^t dt_1 \int_0^t dt_2 \int_0^\infty \mathrm{e}^{-\mathrm{iu}(\mathrm{t}_1-\mathrm{t}_2)} \frac{du}{\pi V} \sum_q |V(q)|^2\Lambda(q,u) \\ &\times \left[\frac{1}{\epsilon^2(q,0)} + \frac{T(v_F q t_1)}{\epsilon(q,0)} + \frac{T(v_F q t_2)}{\epsilon(q,0)} + T(v_F q t_1)T(V_F q t_2)\right] \end{aligned} \tag{2.41}$$

When $t << 1$, then we can find $F_2(t) \approx 0$. It is trivial and has no contribution to the spectral density function. Therefore, the most significant part of the X-ray edge is in the long-time domain. Since the function $T(v_F q t)$ decays very fast, $T(v_F q t_1)T(v_F q t_2)$ is negligible compared to other terms in the bracket, and it implies that

$$\begin{aligned} F_2(t) &\approx \frac{1}{2}\int_0^t dt_1 \int_0^t dt_2 \int_0^\infty \mathrm{e}^{-\mathrm{iu}(\mathrm{t}_1-\mathrm{t}_2)} \frac{du}{\pi V} \sum_q \left[\frac{1}{\epsilon^2(q,0)} + \frac{T(v_F q t_1)}{\epsilon(q,0)} + \frac{T(v_F q t_2)}{\epsilon(q,0)}\right] \\ &\times |V(q)|^2\Lambda(q,u) \\ &= F_2^0(t) - \frac{gu\epsilon}{2}\int_0^t dt_1 \int_0^t dt_2 \int_0^\infty \mathrm{e}^{-\mathrm{iu}(\mathrm{t}_1-\mathrm{t}_2)} du \int_1^\infty \frac{aH_{-1}(u\omega t_1)\sqrt{\omega^2-1}}{\omega\left(\omega^2-1+a^2\right)} d\omega \\ &- \frac{gu\epsilon}{2}\int_0^t dt_1 \int_0^t dt_2 \int_0^\infty \mathrm{e}^{-\mathrm{iu}(\mathrm{t}_1-\mathrm{t}_2)} du \int_1^\infty \frac{aH_{-1}(u\omega t_2)\sqrt{\omega^2-1}}{\omega\left(\omega^2-1+a^2\right)} d\omega \end{aligned} \tag{2.42}$$

In the long time limit, we can extend t into infinity, and then one can get

$$\begin{aligned} F_2(t) &\approx F_2^0(t) + \int_{i/t}^{\xi_0} \frac{2g\epsilon}{\pi u} du \int_1^\infty \frac{a\log(\omega+\sqrt{\omega^2-1})}{\omega^2\left(\omega^2-1+a^2\right)} d\omega \\ &\approx \log(1+g_1 i\xi_0 t) \end{aligned} \tag{2.43}$$

with

$$g_1 = g + \int_1^\infty \frac{2g\epsilon}{\pi} \frac{a\log(\omega+\sqrt{\omega^2-1})}{\omega^2\left(\omega^2-1+a^2\right)} d\omega, \tag{2.44}$$

and $\xi_0 = \frac{\hbar v_F}{2d}$, which is obtained from the previous steps. If graphene is suspended in vacuum, then g=0.25, and $g_1 \approx 0.40$. For graphene suspend

on SiO_2, the coupling constant g is about 0.13, and $g_1 \approx 0.18$. As depicted in Fig 2.1, one can see that the dynamic screening effects of intrinsic graphene significantly change the coupling constant at a small dielectric constant, and this can be understood intuitively. For intrinsic graphene, the Fermi energy is zero, so there is no intrinsic time scale. For long wavelength scattering, the screening time is about $1/(v_F q)$, comparable to the time scale near the edge, so we cannot regard the electrons as completed screened near the edge. Hence, the dynamical screening effects have a considerable influence on the coupling constant. Nevertheless, the Fermi energy is non-zero for normal metals and gated or doped graphene, so the static screening is a good approximation near the edge in those cases. In the large dielectric constant limit, one can see from Fig. 2.1(b), the ratio of the dynamic coupling constant and static coupling constant approaches 1. It can be understood from eq. (1.16) and eq. (2.44), when the external dielectric constant is big enough, it makes the dominant contribution to the total dielectric constant.
In conclusion, one may apply gate voltage on the graphene or increase the external dielectric constant to eliminate the dynamic screening effects.

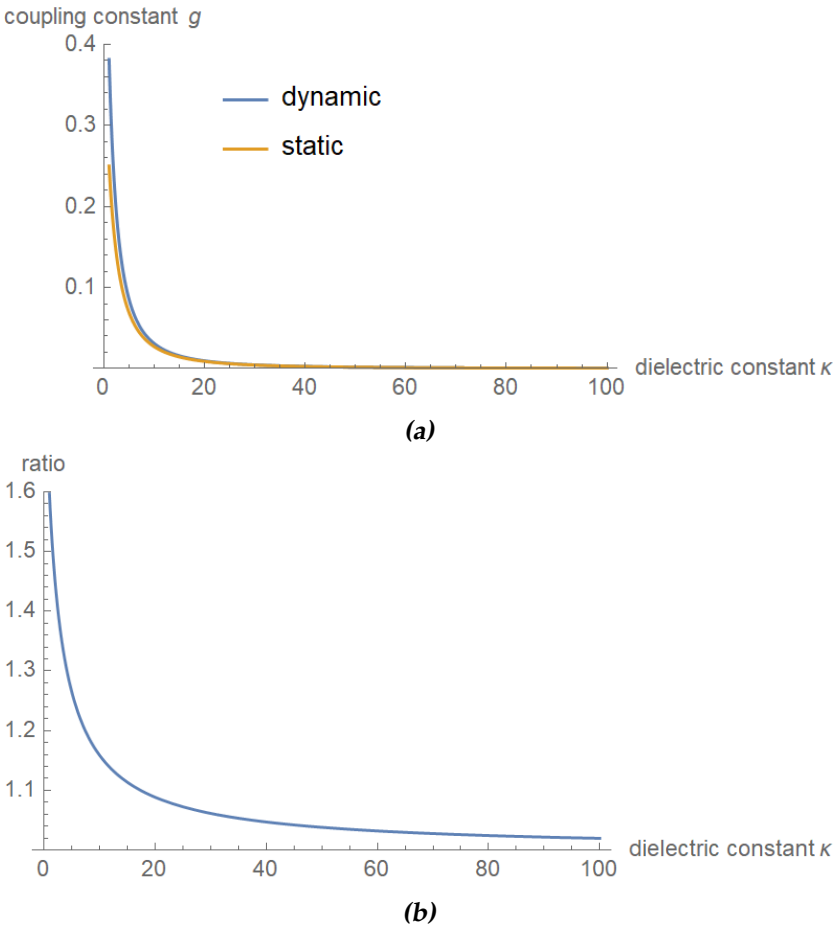

Figure 2.1: *Fig. 2.1(a) depicts the coupling constant with different external dielectric constants. κ describes the dielectric constant of the substrate, and g is the graphene's coupling constant. The blue curve represents the coupling constant considering the dynamic screening effect, and the orange curve representing the coupling constant in the static screening approximation. Fig. 2.1(b) describes the ratio of the dynamic coupling constant and the static coupling constant. In the large dielectric constant limit, the ratio approaches 1.*

Chapter 3

Determinant Method

The previous result is based on the perturbative theory, which neglects the higher-order terms. Usually, it works if the coupling constant of the theory is smaller than 1. However, for freestanding intrinsic graphene, the perturbation theory breaks down if one summarizes all the terms. In the following discussion, we will develop a non-perturbative method, the determinant method, to get a more rigorous result. The result shows that if the dielectric constant of the graphene is big enough, then the perturbative method can give a similar result as in the rigorous non-perturbative method.
The ground state of the Fermi sea can be expressed as

$$|FS\rangle = \frac{1}{\sqrt{N!}}\mathrm{Det}||\psi_i(r_j,\phi_j)|| \tag{3.1}$$

While, the many-body state of the Coulomb problem is

$$|\lambda\rangle = \frac{1}{\sqrt{N!}}\mathrm{Det}||\Psi_i(r_j,\phi_j)|| \tag{3.2}$$

If we use the result in the last line of eq. (1.18), we only need to calculate

$$\left\langle FS \left| e^{-iH_\lambda t/\hbar} \right| FS \right\rangle \mathrm{e}^{iE_0 t/\hbar} \tag{3.3}$$

with $E_0 = \sum_{i,k_i<k_F} \epsilon_i$.
The Hamiltonian H_λ can be expressed as a summation of one-electron

Hamiltonian $\bar{H}_i$. Therefore, expression (3.3) can be expanded as

$$\begin{aligned}\left\langle FS\left|e^{-iH_\lambda t/\hbar}\right|FS\right\rangle \mathrm{e}^{iE_0 t/\hbar} &= \left\langle FS\left|e^{-i\sum_i(\overline{H}_i-\epsilon_i)t/\hbar}\right|FS\right\rangle \\ &= \frac{1}{N!}\sum_{p,p'}(-1)^{p+p'}\prod_i^N\int \psi_i^\dagger(r_{p(i)},\phi_{p(i)})e^{-i(\overline{H}_i-\epsilon_i)t/\hbar} \\ &\times \psi_i(r_{p'(i)},\phi_{p'(i)})d\tau_i\,,\end{aligned} \tag{3.4}$$

where p and p' are any permutations of the N wave vectors. For two different sets of permutations

$$\begin{aligned}p_1 &= \{\cdots i\cdots j\cdots\} \\ p_1' &= \{\cdots j\cdots i\cdots\}\end{aligned} \tag{3.5}$$

and

$$\begin{aligned}p_2 &= \{\cdots j\cdots i\cdots\} \\ p_2' &= \{\cdots i\cdots j\cdots\}\end{aligned} \tag{3.6}$$

we find that

$$\begin{aligned}&(-1)^{p_1+p_1'}\psi_1^\dagger\left(r_{p_1(1)},\phi_{p_1(1)}\right)\mathrm{e}^{-i(\overline{H}_1-\epsilon_1)t/\hbar}\psi_1\left(r_{p_1'(1)},\phi_{p_1'(1)}\right)d\tau_1\times\cdots\times \\ &\psi_i^\dagger\left(r_i,\phi_i\right)\mathrm{e}^{-i(\overline{H}_i-\epsilon_i)t/\hbar}\psi_i\left(r_j,\phi_j\right)d\tau_i\times\cdots\times\psi_j^\dagger\left(r_j,\phi_j\right)\mathrm{e}^{-i(\overline{H}_j-\epsilon_j)t/\hbar}\times \\ &\psi_j\left(r_i,\phi_i\right)d\tau_j\times\cdots \\ &=(-1)^{p_1+p_1'}\psi_1^\dagger\left(r_{p_1(1)},\phi_{p_1(1)}\right)\mathrm{e}^{-i(\overline{H}_1-\epsilon_1)t/\hbar}\psi_1\left(r_{p_1'(1)},\phi_{p_1'(1)}\right)d\tau_1\times\cdots\times \\ &\psi_i^\dagger\left(r_i,\phi_i\right)\mathrm{e}^{-i(\overline{H}_i-\epsilon_i)t/\hbar}\psi_j\left(r_i,\phi_i\right)d\tau_i\times\cdots\times\psi_j^\dagger\left(r_j,\phi_j\right)\mathrm{e}^{-i(\overline{H}_j-\epsilon_j)t/\hbar} \\ &\psi_i\left(r_j,\phi_j\right)d\tau_j\times\cdots \\ &=(-1)^{p_2+p_2'}\psi_1^\dagger\left(r_{p_2(1)},\phi_{p_2(1)}\right)\mathrm{e}^{-i(\overline{H}_1-\epsilon_1)t/\hbar}\psi_1\left(r_{p_2'(1)},\phi_{p_2'(1)}\right)d\tau_1\times\cdots\times \\ &\psi_i^\dagger\left(r_j,\phi_j\right)\mathrm{e}^{-i(\overline{H}_i-\epsilon_i)t/\hbar}\psi_j\left(r_j,\phi_j\right)d\tau_j\times\cdots\times\psi_j^\dagger\left(r_i,\phi_i\right)\mathrm{e}^{-i(\overline{H}_j-\epsilon_j)t/\hbar} \\ &\psi_i\left(r_i,\phi_i\right)d\tau_i\times\cdots \\ &=(-1)^{p_2+p_2'}\psi_1^\dagger\left(r_{p_2(1)},\phi_{p_2(1)}\right)\mathrm{e}^{-i(\overline{H}_1-\epsilon_1)t/\hbar}\psi_1\left(r_{p_2'(1)},\phi_{p_2'(1)}\right)d\tau_1\times\cdots\times \\ &\psi_i^\dagger\left(r_j,\phi_j\right)\mathrm{e}^{-i(\overline{H}_i-\epsilon_i)t/\hbar}\psi_i\left(r_i,\phi_i\right)d\tau_i\times\cdots\times\psi_j^\dagger\left(r_i,\phi_i\right)\mathrm{e}^{-i(\overline{H}_j-\epsilon_j)t/\hbar} \\ &\psi_j\left(r_j,\phi_j\right)d\tau_j\times\cdots\end{aligned} \tag{3.7}$$

The result suggests that for any permutations p and p', the summation in the eq. (3.4) only depends on $p + p'$. Hence, they have the same value for the terms with an equal value of $(-1)^{p+p'}$. Therefore, we get $N!$ duplicated terms in the summation, and they cancel the $N!$ in the denominator of eq. (3.4). Thus, eq. (3.4) can be cast in a straightforward form.

$$\left\langle FS \left| e^{-iH_\lambda t/\hbar} \right| FS \right\rangle \mathrm{e}^{iE_0 t/\hbar} = \mathrm{Det}||\Pi_{ij}|| \tag{3.8}$$

where

$$\Pi_{ij} = \int \psi_i^\dagger(r,\phi)\mathrm{e}^{-i(\overline{H}-\epsilon_i)t/\hbar}\psi_j(r,\phi)d\tau \tag{3.9}$$

If we insert the eigenstate of $\bar{H}$, then we can express the matrix element Π_{ij} in terms of the overlap between the initial one-electron state and the final state. Let χ_p^k be the overlap of ψ_p and Ψ_k. The eq. (3.9) thus becomes

$$\Pi_{kk'} = \sum_p \chi_k^p \chi_{k'}^{p*} \mathrm{e}^{-i(\overline{\epsilon_p}-\epsilon_k)t/\hbar} \tag{3.10}$$

where

$$\chi_k^p = \int \psi_k^* \Psi_p d\tau \tag{3.11}$$

and $\bar{\epsilon}_k$ is the eigen energy of the single Hamiltonian $\bar{H}, \epsilon_p$is the eigen energy of the single Hamiltonian H. The overlap satisfies the normalization condition,

$$\sum_k |\chi_k^p|^2 = 1. \tag{3.12}$$

From eq. (3.10), we can immediately find that $\Pi_{pp'} = \delta_{pp'}$ when $t = 0$. Therefore, we can separate the matrix into a singular part and a smooth part.

$$\Pi = \mathrm{I} - \mathrm{X} \tag{3.13}$$

where

$$X_{kk'} = \sum_p \chi_k^p \chi_{k'}^{p*} (1 - e^{-i(\overline{\epsilon_p}-\epsilon_k)t/\hbar}) \tag{3.14}$$

eq. (3.14) is the most important result for our calculation.
Then, our next step is to calculate the value of $\mathrm{Det}|\mathrm{I} - \mathrm{X}|$. Using Fredholm determinant method [48, 49], we can find that

$$\begin{aligned} \mathrm{Det}|\mathrm{I} - \mathrm{X}| &= \exp(\log(\mathrm{Det}|\mathrm{I} - \mathrm{X}|) = \exp(\mathrm{Tr}\log(\mathrm{I} - \mathrm{X})) \\ &= \exp(-\sum_{\mathrm{k}=1} \frac{\mathrm{TrX^k}}{\mathrm{k}}). \end{aligned} \tag{3.15}$$

Version of July 12, 2021– Created July 12, 2021 - 12:37

3.1 Result for metal

For metal, we obtain the X matrix element in eq. (5.30),

$$X_{kk'} = \frac{\sin\delta_k e^{-i\delta_k}}{\pi\nu_k}\frac{1-e^{-i(\epsilon_{k'}-\epsilon_k)t/\hbar}}{\epsilon_k-\epsilon_{k'}} \tag{3.16}$$

and the details are in Appendix A3. Using the method in reference [24, 50], one can get the asymptotic result of the determinant.

$$\mathrm{Det}|\mathrm{I}-\mathrm{X}| = \exp\left[-it\int_0^\mu \frac{\delta(\epsilon)}{\pi}d\epsilon - \frac{\delta^2(\mu)}{\pi^2}\log(1+i\xi_0 t)\right] \tag{3.17}$$

The first term in the exponent is the self-energy term according to Fumi's theorem [25]. The logarithm part is the origin of infrared catastrophe, and it has the same form as the previous result eq. (1.36). Taking into account the spin degeneracy, the coupling constant is

$$g = 2\frac{\delta^2(\mu)}{\pi^2}. \tag{3.18}$$

One can get the phase shift using eq. (2.25). For metals, based on the equation

$$1/\tau = n_i v\sigma \tag{3.19}$$

and the expression of electron's scattering cross section in three and two dimensions [25, 51, 52], we express eq. (2.25) in the form,

$$\frac{\hbar}{\tau_k} = \frac{2n_i}{\rho(k)\pi}\sin^2\delta(k) \tag{3.20}$$

where $\rho(k)$ is the density of state per spin channel, and it has the explicit form as

$$\rho(k) = \begin{cases} \frac{mk}{2\pi^2\hbar^2}, & \textit{three dimension} \\ \frac{m}{2\pi\hbar^2}, & \textit{two dimension}. \end{cases} \tag{3.21}$$

Under relaxation time approximation [33, 53], we have

$$\frac{\hbar}{\tau_k} = 2\pi\frac{n_i}{L^d}\sum_{k'}|V_{kK'}|^2\delta(\epsilon_{k'}-\epsilon_k)(1-\cos\theta) \tag{3.22}$$

Because $\delta_-(\mu) \ll 1$, the difference between $\sin\delta_-(\mu)$ and $\delta_-(\mu)$ is negligible, i. e. $\delta_-(\mu) \approx \sin\delta_-(\mu)$. Substituting eq. (3.20) and eq. (3.22) into eq. (3.18), one can thus obtain the coupling constant

$$g = 2\rho(E_F)\sum_k |V_{kk_F}|^2\delta(E_F-\epsilon_k)(1-\cos\theta), \tag{3.23}$$

where θ is the angle between $\vec{k_F}$ and $\vec{k}$. In three dimensions, the coupling constant is

$$\begin{aligned} g &= \rho^2(E_F)\int_0^{\pi} d\theta |V(q)|^2 \sin\theta(1-\cos\theta) \\ &\approx 2\rho^2(E_F)V^2(0), \end{aligned} \tag{3.24}$$

and in two dimensional

$$\begin{aligned} g &= 2\frac{\rho^2(E_F)}{2\pi}\int_0^{2\pi} d\theta |V(q)|^2(1-\cos\theta) \\ &\approx 2\rho^2(E_F)V^2(0) \end{aligned} \tag{3.25}$$

where $V(0)$ is the screened potential at Fermi level and $q = 2k_F \sin\frac{\theta}{2}$. It has the same result as in the previous papers. [26, 50]

3.2 Result for graphene

For graphene, the X matrix element is found in eq. (5.43) and eq. (5.72). For details, see Appendix A4 and A5. Following the same procedure as before, we get a similar result.

$$\mathrm{Det}|\mathrm{I}-\mathrm{X}| = \exp\left[-it\int_0^{\mu}\frac{\delta_-(\epsilon)}{\pi}d\epsilon - \frac{\delta_-^2(\mu)}{\pi^2}\log(1+i\xi_0 t)\right] \tag{3.26}$$

If we consider the spin and valley degeneracy, we should add a factor of four before the logarithm term. Therefore, the coupling constant is

$$g = \frac{4\delta_-^2(\mu)}{\pi^2} \tag{3.27}$$

The phase shift can be obtained from eq. (2.25). For Coulomb potential, we can evaluate the mean free time under relaxation time approximation [54–56].

$$\frac{\hbar}{\tau} = n_i\frac{\rho(E_F)}{8}\int_0^{2\pi} d\theta |V(q)|^2(1-\cos^2\theta) \tag{3.28}$$

$$q = 2k_F\sin\frac{\theta}{2} \tag{3.29}$$

Under RPA approximation, the Coulomb potential becomes

$$V(q) = \frac{2\pi \mathrm{e}^2 \mathrm{e}^{-\mathrm{qd}}}{\epsilon q} \tag{3.30}$$

Version of July 12, 2021– Created July 12, 2021 - 12:37

Substituting it into the eq. (3.28), we have

$$\frac{\hbar}{\tau} = \left(\frac{2\pi e^2}{\epsilon}\right)^2 \frac{\rho(E_F)}{8k_F^2} \frac{\pi \left(I_1(4dk_F) - L_1(4dk_F)\right)}{2dk_F} \tag{3.31}$$

Comparing the result with eq. (2.25), it gives

$$\sin^2 \delta_-(\mu) = \frac{e^4 \pi^2}{4\epsilon^2 \hbar^2 v_F^2} \frac{I_1(4dk_F) - L_1(4dk_F)}{2dk_F} \tag{3.32}$$

Because $\delta_-(\mu) \ll 1$, the difference between $\sin \delta_-(\mu)$ and $\delta_-(\mu)$ is negligible, i. e. $\delta_-(\mu) \approx \sin \delta_-(\mu)$. Taking into account the spin and valley degeneracy, we find the coupling constant g is

$$g = \frac{e^4}{\epsilon^2 \hbar^2 v_F^2} \frac{I_1(4dk_F) - L_1(4dk_F)}{2dk_F} \tag{3.33}$$

In the clean limit, $k_F = 0$ for intrinsic graphene, so we have

$$\lim_{k_F \to 0} g = g = \frac{e^4}{\epsilon^2 \hbar^2 v_F^2}, \tag{3.34}$$

where we use the following equality

$$\lim_{k_F \to 0} \frac{I_1(4dk_F) - L_1(4dk_F)}{2dk_F} = 1 \tag{3.35}$$

The result in eq. (3.34) is the same as in the eq. (1.35). So one can conclude that the coupling constant obtained in the linked cluster expansion coincides with the result in the determinant method if one only keeps the first-order term of the phase shift under the born approximation. The cut-off energy can be got from the approximation that the exponent in the integral of eq. (3.28) can be neglected, i. e., $\exp(-2qd) \approx 1$. Hence, we can get a rough estimation of it.

$$\xi_0 = \frac{\hbar v_F}{2d}. \tag{3.36}$$

From rigorous derivation [57–59], one can find the expression of the phase shifts due to the Coulomb scattering.

$$e^{2i\delta_{js}} = \frac{j}{\gamma + is\alpha} \frac{\Gamma(1 + \gamma + is\alpha)}{\Gamma(1 + \gamma - is\alpha)} e^{i\pi(j-\gamma)} \tag{3.37}$$

s is the sign for the band index, j is the total angular momentum number, and it is $1/2$ for s wave. α is the effective fine structure constant of graphene,

$$\alpha = \frac{e^2}{4\pi\epsilon_0\epsilon\hbar v_F}. \tag{3.38}$$

The definition of γ is

$$\gamma = \sqrt{j^2 - \alpha^2} \tag{3.39}$$

If graphene is suspended in a vacuum, we can calculate the phase shift numerically. In that case, $\alpha \approx 1/2$, thus phase shift for s wave scattering is $\delta \approx \pi/2$, and one can also obtain that the coupling constant $g \approx 1$, which invalidate the perturbative theory. Also, if graphene is suspended on SiO_2, then the coupling constant is about 0.20. As depicted in Fig. 3.1(a) and Fig. 3.1(b), perturbative method does not work well if the external dielectric constant κ is not big enough. This phenomenon can be understood from the following aspects. As we mentioned before, the linked cluster expansion results can be recovered under the Born approximation. However, the Born approximation is only valid for short-range potential, breaking down for the long-range Coulomb potential. Although we cannot consider the dynamical screening effects in this method, we can rule them out if we apply the substrate of a very high dielectric constant from the previous discussion. One may include the disorder effects in this method, but the calculation would be more complicated than the linked cluster expansion. However, from the previous result, we know that we can neglect the disorder effects if the disorder concentration is not big enough.
Overall, the determinant method gives a more rigorous result than the linked cluster expansion does. The result is valuable for the experimental physicists since the determinant method gives a more accurate relation between the coupling constant and the external dielectric constant.

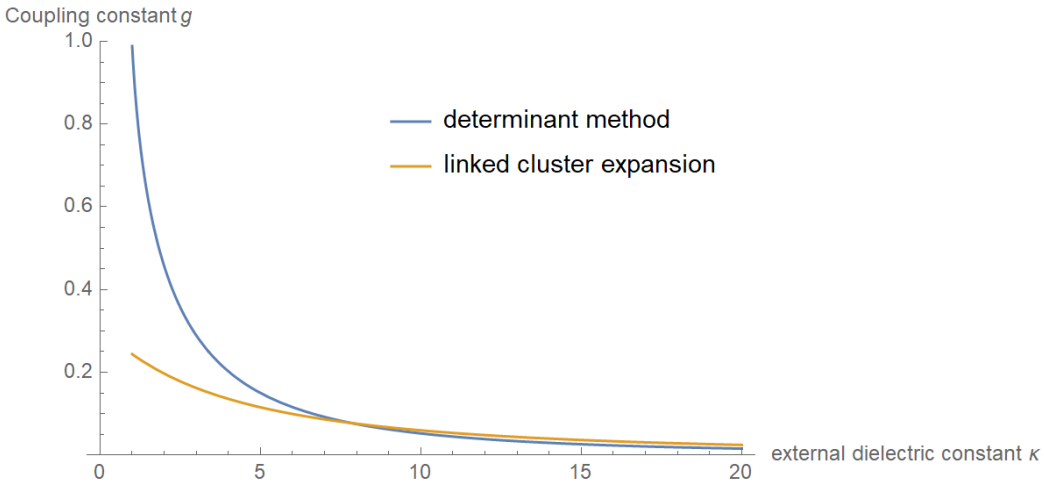

(a)

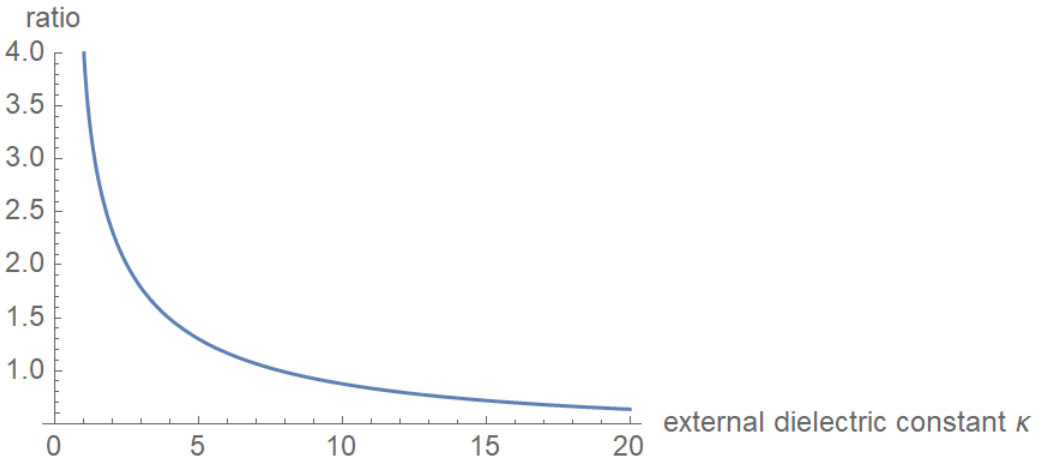

(b)

Figure 3.1: *Fig. 3.1(a) depicts the coupling constant at different external dielectric constants. For freestanding graphene, the dielectric constant is 1. Fig. 3.1(b) depicts the ratio of coupling constants obtained in two different methods. Even in the large external dielectric constant limit, the results obtained in two different methods are not the same.*

Chapter 4

Conclusion and Outlook

4.1 Conclusion

4.1.1 Relevance to the Ptolemy Project

In this section, we will show the results directly related to the Ptolemy project. From eq. (1.19), we know that we can get the smeared beta decay spectrum by performing a convolution between the spectral density function and the beta decay spectrum. Using Mathematica, we plotted the zero lightest neutrino mass figures, namely $m_{lightest} = 0$. As indicated in Fig. 4.1(a) and Fig. 4.1(b), the cosmic neutrino background spectrum will be broadened by the power-law decay behavior of the spectral density function. From the smeared spectrum, we can obtain the visibility of the Ptolemy project, namely, the non-overlap region in the spectrum. One can draw a contour plot of the visibility. As shown in Fig. 4.2, the smaller the coupling constant is and the larger the lightest mass of the neutrino is, the higher visibility that the Ptolemy project has. This result can be explained by the fact that a large coupling constant leads to a sharper distribution, which causes the beta decay spectrum less broadening.
Apart from the coupling constant, the cutoff energy also influences the visibility of the Ptolemy project. Fig. 4.3 describes the dependence of the Ptolemy project's visibility on the distance d, i. e., the cutoff energy. Smaller scale parameter, i. e. more oversized height d means less weighted in the long tail of the gamma distribution, which leads to a less broadening spectrum. Therefore, as depicted in Fig. 4.3 at a specific coupling constant and the lightest mass of the neutrino, the visibility increases with the helium ion's height.

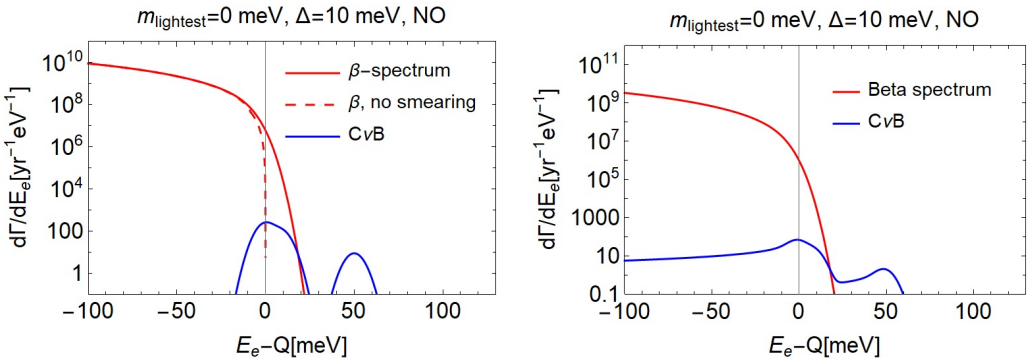

(a) *original beta decay spectrum when the lightest neutrino mass equals zero.*

(b) *smeared beta decay spectrum*

Figure 4.1: *Fig. 4.1(a) is the original beta decay spectrum when the lightest neutrino mass equals zero. The solid red curve represents the background beta decay. The dashed red line represents the background beta decay spectrum with the smearing of Gaussian distribution caused by the finite experimental resolution, namely $\Delta = 10meV$. The solid blue curve represents the cosmic neutrino background that is the signal we want to detect. $d\Gamma/dE$ describes the possibility that the events happen at a given energy per year. The area under the curve represents the number of events per year. The area under the blue curve is only four, which means we can only detect at most four cosmic neutrinos per year. The noise of background beta decay covers the overlap between the red curve and blue curve, and it means we cannot distinguish whether the source of the signals comes from the cosmic neutrino or background beta decay. Fig. 4.1(b) describes the smeared beta decay spectrum. We choose the coupling constant g=0.25.*

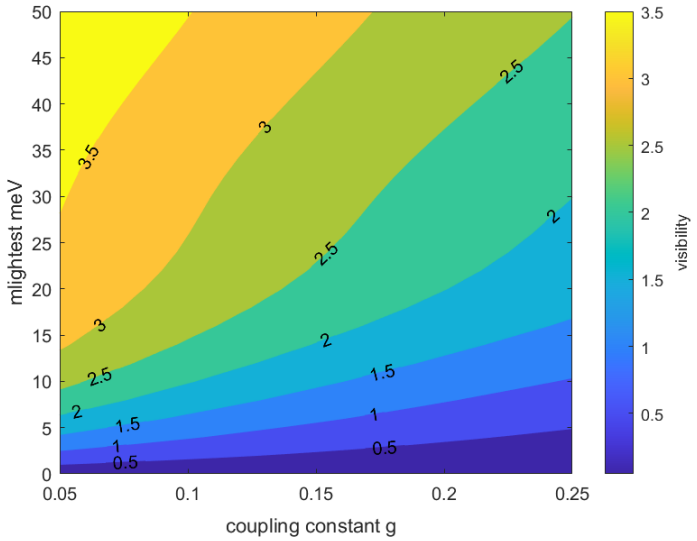

Figure 4.2: *Contour plot of visibility with the different lightest mass of the neutrino and coupling constant when the cut-off energy is 1 eV. The total area under the CNB curve is 4.*

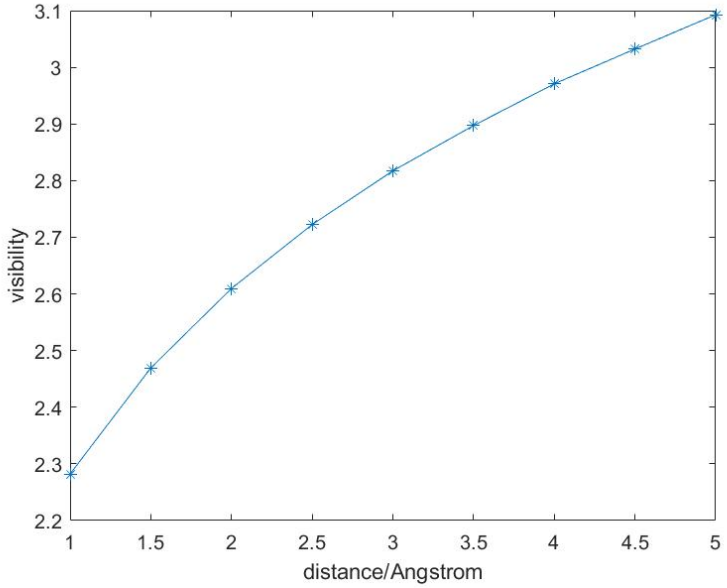

Figure 4.3: *Visibility at different heights with coupling constant g= 0.2, and* $m_{lightest} = 50meV$. *The curves with different coupling constants and the neutrinos' lightest mass share a similar feature.*

4.1.2 Overview of this work

In this work, we discussed how the X-ray edge in the graphene influences the visibility of the Ptolemy project. In the first chapter, we used Fermi's golden rule to find the smeared beta decay spectrum. We found out that it is the convolution between the spectral density function of graphene and the original beta decay spectrum function. Moreover, we apply the perturbation theory, linked cluster expansion, to obtain the spectral density function, which is precisely the gamma distribution function and controlled by the cutoff energy and coupling constant
In the second chapter, we examined factors that influence the coupling constant and the cutoff energy. We found natural distance-dependent cutoff energy by considering the height of the helium ion. Also, the disorder effects can be ruled out if the concentration of the tritium atom is less than $5 \times 10^{11}/cm^2$. However, the dynamic screening effects of the intrinsic graphene significantly enlarge the coupling constant, which decreases the visibility of the Ptolemy project. Fortunately, if the external dielectric constant of the substrate is big enough, the dynamic screening effects can be eliminated. Moreover, we also found the spectral density function of the simple metal such as gold foil, and it has the same form as in the graphene but with a fixed coupling constant and cutoff energy. We can neglect the disorder effect for simple metals because of the enormous amount of electrons in metals.
In the next chapter, we developed the determinant method to obtain a more rigorous dependence of the coupling constant on the external dielectric constant for the graphene deposited on a low-dielectric-constant substrate. This result can help the experimental physicists to find the proper substrate to increase the Ptolemy project's visibility.

4.1.3 Suggestions to Ptolemy Collaboration

In conclusion, we suggest that there are two options to improve the visibility of the Ptolemy project:
(1) find a substrate with a high dielectric constant;
(2) increase the height of tritium atoms from the graphene sheet.
Besides, metal is not a good choice for tritium target substrate.

4.2 Outlook

Although we have considered several effects that can affect the spectral density function, several effects still require further study. For instance, the finite lifetime of the helium ion may cause a Lorentz broadening in the spectrum, which may eliminate the X-ray edge. We only explore the X-ray edge problem in the ungated graphene, but the emergent phenomena in the gated graphene may influence the X-ray edge problem. Gating can eliminate the dynamic screening effect near the edge, so it can decrease the coupling constant. However, there is no free lunch. Gating may cause some annoying effects, such as inhomogeneous broadening [60].
Moreover, in section 2.3, we discussed the disorder effects in the metallic regime. However, tritium's coverage is too small in the metallic regime to provide a high number density. If the coverage of tritium increases, the graphene undergoes a metal-insulator transition. In the insulating regime, tritium atoms can open a small bandgap for the tritiated graphene. The bandgap can change the dispersion relationship of the electrons and the density response function of electrons in graphene. Therefore, the X-ray edge in the insulating regime is more complicated, and we will leave the related problems in further study.

Version of July 12, 2021– Created July 12, 2021 - 12:37

Chapter 5

Appendix

5.1 A1

If we consider the helium ion is static, then the Hamiltonian of the graphene can be expressed as

$$\begin{aligned} H_\lambda &= \sum_s \int d^2x \psi_s^\dagger(x) \cdot (-i\hbar v_F \vec{\nabla} \cdot \vec{\sigma}) \cdot \psi_s(x) + H_{h-g} \\ &= \sum_s \int d^2x \psi_s^\dagger(x) \cdot (-i\hbar v_F \vec{\nabla} \cdot \vec{\sigma}) \cdot \psi_s(x) - \int \frac{e^2}{4\pi\epsilon\epsilon_0} \frac{\rho(x) h_0^\dagger h_0}{\sqrt{d^2+x^2}} d^2x \end{aligned} \tag{5.1}$$

The state $|\lambda\rangle$ is the eigenstate of it. The eigenstate should be a tensor product of the electron state of graphene and helium ion state. However, only the graphene part of the eigenstate is important to our calculation so that we can neglect the ladder operators of Helium ion in the Hamiltonian H_λ. Thus, the Hamiltonian H_λ can be expressed as

$$H_\lambda = \sum_s \int d^2x \psi_s^\dagger(x) \cdot (-i\hbar v_F \vec{\nabla} \cdot \vec{\sigma}) \cdot \psi_s(x) - \int \frac{e^2}{4\pi\epsilon\epsilon_0} \frac{\rho(x)}{\sqrt{d^2+x^2}} d^2x \tag{5.2}$$

We can express the Hamiltonian H_λ in the momentum space.

$$\begin{aligned}
H_\lambda &= \sum_s \int d^2x \sum_k \psi^\dagger_{ks} \frac{\mathrm{e}^{-i\vec{k}\vec{x}}}{L} C^\dagger_{ks}(-i\hbar v_F) \cdot \begin{pmatrix} 0 & \partial_x - i\partial_y \\ \partial_x + i\partial_y & 0 \end{pmatrix} \sum_{k'} \psi_{k's} \frac{\mathrm{e}^{-i\vec{k}\vec{x}}}{L} \\
&\times C_{k's} - \int \frac{e^2 d^2x}{4\pi\epsilon\epsilon_0\sqrt{d^2+x^2}} : \sum_{ks} \psi^\dagger_{ks} \frac{\mathrm{e}^{-i\vec{k}\vec{x}}}{L} C^\dagger_{ks} \sum_{k's'} \psi_{k's'} \frac{\mathrm{e}^{-i\vec{k}\vec{x}}}{L} C_{k's'} : h^\dagger_0 h_0 \\
&= \sum_{s,k,k'} \delta_{k,k'} s\hbar v_F k C^\dagger_{ks} C_{k's} - \sum_{s,s',k,k'} \frac{e^2 \psi^\dagger_{k\delta} \psi_{k's'} \sum_l i^l J_l[(\vec{k'}-\vec{k})\vec{x}] \mathrm{e}^{il\varphi} x dx d\varphi}{4\pi\epsilon\epsilon_0 L^2 \sqrt{d^2+x^2}} \\
&\times C^\dagger_{ks} C_{k's'} h^\dagger_0 h_0 \\
&= \sum_{k,s} s\hbar v_F k C^\dagger_{ks} C_{ks} - \sum_{s,s'} \sum_{kk'} F_{ss'}(k,k') \frac{e^2 \exp\left(-|k'-k|d\right)}{2\epsilon\epsilon_0 L^2 |k-k'|} C^\dagger_{ks} C_{k's'} h^\dagger_0 h_0
\end{aligned} \tag{5.3}$$

where L^2 is the area of graphene. The spinor takes the form as [61]

$$\psi_{ks} = \frac{1}{\sqrt{2}} \begin{pmatrix} e^{-i\theta_k} \\ s \end{pmatrix} \tag{5.4}$$

with $\theta_k = \arctan(k_y/k_x)$.
$F_{ss'}(k,k')$ is regarded as the overlap between the two spinors, and it is expressed as

$$F_{ss'}(k,k') = \frac{1}{2}\left[ss' + \exp(i\theta_k - i\theta_{k'})\right] \tag{5.5}$$

The Coulomb-type potential is only valid in the long range, and the potential behaves smoothly in the short range. Therefore, the Coulomb-type potential can only be valid up to cutoff energy, say, ξ_0. This assumption will help us to reduce the complexity of the problem. To simplify the problem, naively, we can get rid of the factor $\exp\left(-|k-k'|d\right)$. It is quite crude to make such an approximation, but it is valid near the x-ray singularity edge, i. e., a tiny wave vector. For our problem, the dominant contribution comes from the X-ray singularity edge since the initial state and final state have considerable overlap in this region. Then, we reduce the potential to a familiar 2D Coulomb potential.

$$\begin{aligned}
H_\lambda &= \sum_s \sum_k s\hbar v_F k C^\dagger_{ks} C_{k's} - \sum_{ss'} \sum_{kk'} \frac{e^2 F_{ss'}(k,k')}{2\epsilon\epsilon_0 L^2 |k-k'|} C^\dagger_{ks} C_{k's'} h^\dagger_0 h_0 \\
&= \sum_s \sum_k s\hbar v_F k C^\dagger_{ks} C_{k's} - \frac{1}{L^2} \sum_{ss'} \sum_{kk'} V(k,k') F_{ss'}(k,k') C^\dagger_{ks} C_{k's} h^\dagger_0 h_0
\end{aligned} \tag{5.6}$$

Version of July 12, 2021– Created July 12, 2021 - 12:37

5.2 A2

To find $\Lambda(q,u)$, we need to obtain the explicit form of the polarizability function $P^{(1)}(q,u)$ first. For intrinsic graphene, the Green's function is

$$G_{ss}(p,E) = \frac{1}{E - \xi_{sp} + i\eta_p} \tag{5.7}$$

η_p is an infinitesimal quantity whose sign depends on the sign of ξ_{sp}. The negative sign is for $\xi_{sp} < 0$, and the positive sign is for $\xi_{sp} > 0$. Inserting the Green function into the eq. (1.33), one can obtain that

$$\begin{aligned} P^{(1)}(q,u) &= \frac{-ig'}{L^2} \sum_{p,s,s'} \int_{-\infty}^{\infty} \frac{dE}{2\pi} \frac{F_{ss'}(p,p+q)}{E+u-\xi_{s'(p+q)}+i\eta_{p+q}} \frac{1}{E-\xi_{sp}+i\eta_p} \\ &= \frac{-ig'}{L^2} \sum_{p,s,s'} \frac{F_{ss'}(p,p+q)}{u+\xi_{sp}-\xi_{s'(p+q)}+i\eta} \int_{-\infty}^{\infty} \frac{dE}{2\pi} \\ &\times \left[\frac{1}{E-\xi_{sp}+i\eta_p} - \frac{1}{E+u-\xi_{s^{prime}(p+q)}+i\eta_{p+q}} \right] \\ &= \frac{g'}{L^2} \sum_{p,s,s'} F_{ss'}(p,p+q) \frac{f_{sp} - f_{s'(p+q)}}{u+\xi_{sp}-\xi_{s'(p+q)}+i\eta} \end{aligned} \tag{5.8}$$

The imaginary part of the polarizability function, $P^{(1)}(q,u)$, gives $\Lambda(q,u)$.

$$\Lambda(q,u) = \frac{\pi g_s g_\nu}{L^2} \sum_{pss'} |F_{ss'}(p,p+q)|^2 \left(f_{sp} - f_{s'(p+q)}\right) \delta(u + \xi_{sp} - \xi_{s'(k+q)}) \tag{5.9}$$

$$|F_{ss'}(p,p+q)|^2 = \frac{1-\cos(\theta_{p,p+q})}{2}. \tag{5.10}$$

At zero temperature, the non-zero term is

$$\Lambda(q,u) = \frac{\pi g_s g_\nu}{2L^2} \sum_k \left(1 - \cos(\theta_{p,p+q})\right) \delta(u - \xi_p - \xi_{p+q}) \tag{5.11}$$

We can express the $\theta_{k,k+q}$ in terms of the angle between $\vec{k}$ and $\vec{q}$.

$$\Lambda(q,u) = \frac{\pi g_s g_\nu}{2L^2} \sum_p \left(1 - \frac{p + q\cos\varphi}{|\vec{p}+\vec{q}|}\right) \delta(u - \xi_p - \xi_{p+q}) \tag{5.12}$$

Version of July 12, 2021– Created July 12, 2021 - 12:37

Changing the sum into integral, we can then evaluate it.

$$\begin{aligned}
\Lambda(q,u) &= 2\frac{\pi g_s g_\nu}{2(2\pi)^2}\int_0^\infty pdp\int_0^\pi d\varphi(1-\frac{p+q\cos\varphi}{|\vec{p}+\vec{q}|})\frac{\delta(\varphi-\varphi_0)}{v_F|\frac{pq\sin\varphi_0}{|\vec{p}+\vec{q}|}|}\\
&= \frac{g_s g_\nu}{4\pi}\int_0^\infty pdp\frac{u-v_Fp-v_Fp-(u^2-v_F^2q^2-2uv_Fk)/(2v_Fp)}{\sqrt{4v_F^4p^2q^2-(u^2-v_F^2q^2-2uv_Fp)^2}/2}\\
&= \frac{g_s g_\nu}{4\pi}\int_0^\infty dp\frac{4uv_Fp-4v_F^2p^2-(u^2-v_F^2q^2)}{v_F\sqrt{(u^2-v_F^2q^2)(-4v_F^2p^2+4uv_Fp-(u^2-v_F^2q^2))}}\\
&= \frac{g_s g_\nu}{4\pi}\int_0^\infty dp\frac{\sqrt{4uv_Fp-4v_F^2p^2-(u^2-v_F^2q^2)}}{v_F\sqrt{u^2-v_F^2q^2}}\\
&= \frac{g_s g_\nu}{8\pi}\int_{-q}^{q} dp\frac{\sqrt{q^2-p^2}}{\sqrt{u^2-v_F^2q^2}}\Theta(u-v_Fq)\\
&= \frac{g_s g_v}{16}\frac{q^2}{\sqrt{u^2-v_F^2q^2}}\Theta(u-v_Fq)
\end{aligned} \tag{5.13}$$

It matches the results in the references [29]

5.3 A3

To find the overlap between scattering state and incident state, we use the following model to characterize the one-body Hamiltonian.

$$\overline{H} = \sum_k \epsilon_k C_k^\dagger C_k + \frac{1}{V}\sum_{kk'} V_{kk'} C_k^\dagger C_{k'} \tag{5.14}$$

Creation operators characterize the scattering states.

$$\overline{C}_p^\dagger = \sum_{k'} \chi_{k'}^p C_{k'}^\dagger \tag{5.15}$$

The new set of operators obey the equation of motion.

$$[\overline{H}, \quad \overline{C}_p^\dagger] = \overline{\epsilon_p}\,\overline{C}_p^\dagger \tag{5.16}$$

Version of July 12, 2021– Created July 12, 2021 - 12:37

Inserting eq. (5.14) into the equation of motion, it gives

$$\epsilon_{k'}\chi^p_{k'} + \frac{1}{V}\sum_{k''} V_{k'k''}\chi^p_{k''} = \overline{\epsilon_p}\chi^p_{k'} \tag{5.17}$$

The second term is a function about p and k', so we set it as $\eta_{k'p}$. Thus, we can get the expression of the overlap in terms of $\eta_{k'p}$.

$$\chi^p_{k'} = \frac{\eta_{k'p}}{V(\overline{\epsilon_p} - \epsilon_{k'})} \tag{5.18}$$

We can recognize that the coefficient $\eta_{k'p}$ is the T matrix.

$$\eta_{k'p} = \sum_{k''} V_{k'k''}\chi^p_{k''} = \sum_{k''} \langle\psi_{k'}|V(\vec{r})|\psi_{k''}\rangle \langle\psi_{k''}|\Psi_p\rangle = \langle\psi_{k'}|V(\vec{r})|\Psi_p\rangle = T_{k'p} \tag{5.19}$$

The unitary condition of the overlap (eq. (3.12)) gives the equations about $\eta_{pk'}$.

$$\sum_{k'} \frac{|\eta_{k'p}|^2}{V^2(\overline{\epsilon_p} - \epsilon_{k'})^2} = 1 \tag{5.20}$$

The region of $p \approx k'$ controls this equation. We can use the following approximation to get the result.

$$\eta_{k'p} \approx \eta_{pp}, \tag{5.21}$$

$$V(\overline{\epsilon_p} - \epsilon_{k'}) \approx \frac{p - k'}{\nu_p} - \frac{\delta_p}{\pi\nu_p}, \tag{5.22}$$

where ν_p is the density of state at p state, and δ_p is the phase shift at p state. Under those approximations, using the Poisson summation formula, we have

$$\sum_{k'} \frac{\nu_p^2|\eta_{pp}|^2}{(p - k' - \delta_p)^2} = \sum_{Res} -\frac{\nu_p^2|\eta_{pp}|^2\pi\cot\pi k'}{(p - k' - \delta_p)^2} = \frac{\pi^2\nu_p^2|\eta_{pp}|^2}{\sin^2\delta_p} = 1, \tag{5.23}$$

which gives

$$\eta_{k'p} \approx \eta_{pp} = \frac{\sin\delta_p}{\pi\nu_p} \tag{5.24}$$

One can also derive this result from the property of T matrix.

$$T_{k'p} = 4\pi\sum_l (2l+1)P_l(\cos\theta_{k'p})T_l(k', p) \tag{5.25}$$

Version of July 12, 2021– Created July 12, 2021 - 12:37

where $\theta_{k'p}$ is the angle between $\vec{k'}$ and $\vec{p}$. If we only consider elastic s wave scattering, then the T matrix can be cast into a simple expression [25]

$$T_{k'p} = 4\pi T_l(k', p) = -\frac{e^{i\delta_l}\sin\delta_p}{\pi\nu_p}. \tag{5.26}$$

Since the T matrix always shows up in pairs in the Π matrix, those two results are the same for our calculation. Therefore, the overlap can be written as

$$\chi^p_{k'} = \frac{\sin\delta_p}{V\pi\nu_p(\overline{\epsilon_p} - \epsilon_{k'})} \tag{5.27}$$

Instituting it into the expression of matrix element $X_{kk'}$, eq. (3.14), it gives

$$X_{kk'} = \sum_p \frac{\sin^2\delta_p(1 - e^{-i(\overline{\epsilon_p}-\epsilon_k)t/\hbar})}{V^2\pi^2\nu_p^2(\overline{\epsilon_p} - \epsilon_k)(\overline{\epsilon_p} - \epsilon_{k'})} \tag{5.28}$$

Using Pioncaré-Bertrand theorem [62]

$$\begin{aligned} P\frac{1}{(\overline{\epsilon_p} - \epsilon_k)(\overline{\epsilon_p} - \epsilon_{k'})} = P\frac{1}{\epsilon_k - \epsilon_{k'}}\left(\frac{1}{\overline{\epsilon_p} - \epsilon_k} - \frac{1}{\overline{\epsilon_p} - \epsilon_{k'}}\right) \\ + \pi^2\delta(\overline{\epsilon_p} - \epsilon_k)\delta(\overline{\epsilon_p} - \epsilon_{k'}) \end{aligned} \tag{5.29}$$

one can evaluate this expression.

$$\begin{aligned} X_{kk'} &= \sum_p \left[P\frac{1}{\epsilon_k - \epsilon_{k'}}\left(\frac{1}{\overline{\epsilon_p} - \epsilon_k} - \frac{1}{\overline{\epsilon_p} - \epsilon_{k'}}\right) + \pi^2\delta(\overline{\epsilon_p} - \epsilon_k)\delta(\overline{\epsilon_p} - \epsilon_{k'})\right] \\ &\times \frac{\sin^2\delta_p\left(1 - e^{-i(\overline{\epsilon_p}-\epsilon_k)t/\hbar}\right)}{V^2\pi^2\nu_p^2} \\ &= -\sum_{Res} \frac{\sin^2\delta_p\left(1 - e^{-i(\overline{\epsilon_p}-\epsilon_k)t/\hbar}\right)}{V^2\pi^2\nu_p^2(\epsilon_k - \epsilon_{k'})}\left(\frac{1}{\overline{\epsilon_p} - \epsilon_k} - \frac{1}{\overline{\epsilon_p} - \epsilon_{k'}}\right)\pi\cot\pi p \\ &+ \pi^2\delta(\epsilon_k - \epsilon_{k'})\frac{\sin^2\delta_k\left(1 - e^{-i(\epsilon_{k'}-\epsilon_k)t/\hbar}\right)}{V^2\pi^2\nu_k^2} \\ &= \frac{\sin\delta_k\cos(\delta_k)}{\pi\nu_k}\frac{1 - e^{-i(\epsilon_{k'}-\epsilon_k)t/\hbar}}{\epsilon_k - \epsilon_{k'}} - \frac{i\sin\delta_k\sin\delta_k}{\pi\nu_k}\frac{1 - e^{-i(\epsilon_{k'}-\epsilon_k)t/\hbar}}{\epsilon_k - \epsilon_{k'}} \\ &= \frac{\sin\delta_k e^{-i\delta_k}}{\pi\nu_k}\frac{1 - e^{-i(\epsilon_{k'}-\epsilon_k)t/\hbar}}{\epsilon_k - \epsilon_{k'}} \end{aligned} \tag{5.30}$$

Version of July 12, 2021– Created July 12, 2021 - 12:37

In the third step, we use the identity,

$$\lim_{\eta\to 0}\frac{1}{\epsilon_k-\epsilon_{k'}-i\eta}=i\pi\delta(\epsilon_k-\epsilon_{k'}) \tag{5.31}$$

5.4 A4

Assuming the ground state of graphene is in a half-filled state, we only need to consider the valence band. Therefore, the element of the matrix X becomes

$$X_{kk'}=\sum_{ps}\chi^{ps}_{k-}\chi^{ps*}_{k'-}(1-e^{-i(\overline{\epsilon_{ps}}+\epsilon_k)t/\hbar}) \tag{5.32}$$

The spinor-included one-body Hamiltonian of graphene is

$$\overline{H}=\sum_{ks}\epsilon_{ks}C^\dagger_{ks}C_{ks}+\frac{1}{V}\sum_{kk'}\sum_{ss'}V_{kk'}F_{ss'}(k,k')C^\dagger_{ks}C_{k's'}. \tag{5.33}$$

The new set of ladder operators is

$$\overline{C}^\dagger_{ps}=\sum_{k's'}\chi^{ps}_{k's'}C^\dagger_{k's'};\quad \overline{C}_{ps}=\sum_{k's'}\chi^{ps*}_{k's'}C_{k's'}. \tag{5.34}$$

The new equation of motion is

$$[\overline{H},\quad \overline{C}^\dagger_{ps}]=\overline{\epsilon_{ps}}\,\overline{C}^\dagger_{ps}. \tag{5.35}$$

Inserting eq. (5.33) into the equation of motion, it gives

$$\epsilon_{k's'}\chi^{ps}_{k's'}+\frac{1}{V}\sum_{k''s''}V_{k'k''}\chi^{ps}_{k''s''}F_{s's''}(k',k'')=\overline{\epsilon_{ps}}\chi^{ps}_{k's'} \tag{5.36}$$

Solving the equation of motion, we get

$$\chi^{ps}_{k's'}(k',p)=\frac{\eta^{ss'}_{k'p}}{V(\overline{\epsilon_{ps}}-\epsilon_{k's'})} \tag{5.37}$$

where

$$\eta^{ss'}_{k'p}=\sum_{k''s''}V_{k'k''}\chi^{ps}_{k''s''}F_{s's''}(k',k''). \tag{5.38}$$

This complicated tensor η is also the T matrix but depends on the band index. For graphene, the T matrix is expanded in two dimensions.

$$T_{k'p}=2\pi\sum_l\exp(il\theta_{k'p})T_l(k',p) \tag{5.39}$$

Version of July 12, 2021– Created July 12, 2021 - 12:37

where $T_l(k', p)$ is diagonalized [30].

$$T_l(P, P) = \frac{e^{i\delta_p} \sin \delta_p}{2\pi^2 \nu_p} \tag{5.40}$$

For the lowest order scattering, s wave scattering, the T matrix is

$$T_0(p) = \frac{\mathrm{e}^{i\delta_p} \sin \delta_p}{\pi \nu_p}. \tag{5.41}$$

Substituting the solution of the equation of motion eq. (5.37)into the X matrix element eq. (5.32), one can obtain that

$$X_{kk'} = \sum_{ps} \frac{\eta_{kp}^{s-} \eta_{k'p}^{s-*}}{V^2(\overline{\epsilon_{ps}} + \epsilon_k)(\overline{\epsilon_{ps}} + \epsilon_{k'})}(1 - e^{-i(\overline{\epsilon_{ps}} + \epsilon_k)t/\hbar}) \tag{5.42}$$

Since most of the contribution comes from the vicinity of $\overline{\epsilon_{ps}} \approx -\epsilon_k \approx -\epsilon_{k'}$, we can cast the expression eq. (5.42) into a simple way by performing the Poisson summation.

$$X_{kk'} = \frac{\sin \delta_{k-} \mathrm{e}^{-i\delta_{k-}}}{\pi \nu_k} \frac{1 - \mathrm{e}^{i(\epsilon_{k'} - \epsilon_k)t/\hbar}}{\epsilon_{k'} - \epsilon_k} \tag{5.43}$$

5.5 A5

We can derive the above result from a more direct way. The one-body Hamiltonian is

$$\overline{H} = H_0 + \hat{V} \tag{5.44}$$

We can construct the scattering wave by using the superposition of incident wave and outgoing wave.

$$|\Psi_{ks}\rangle = |\phi_{ks}\rangle + \sum_{k's'} \frac{|\phi_{k's'}\rangle \langle \phi_{k's'}| \hat{V} |\Psi_{ks}\rangle}{\epsilon_{ks} - \epsilon_{k's'} + i\eta} \tag{5.45}$$

where $|\phi_{ks}\rangle$ is the incident wave, $|\Psi_{ks}\rangle$ is the scattering wave, η is an infinitesimal quantity. It is easily to verify that the scattering wave is an eigenstate of Hamiltonian $\overline{H}$ with eigen value ϵ_{ks}.
Multiplying both sides of eq. (5.45) by $\langle \phi_{k's'}|$, we can obtain the overlap between the scattering state and the incident state.

$$\begin{aligned} \chi_{k's'}^{ks} &= \delta_{kk'}\delta_{ss'} + \frac{\langle \phi_{k's'}| \hat{V} |\Psi_{ks}\rangle}{\epsilon_{ks} - \epsilon_{k's'} + i\eta} \\ &= \delta_{kk'}\delta_{ss'} + \frac{T_{k'k}^{ss'}}{\epsilon_{ks} - \epsilon_{k's'} + i\eta} \end{aligned} \tag{5.46}$$

It satisfies the unitary condition,

$$\begin{aligned}\sum_{ps''} \chi_{ks}^{ps''} \chi_{k's'}^{ps''*} &= \delta_{kk'}\delta_{ss'} + \frac{T_{kk'}^{ss'}}{\epsilon_{k's'} - \epsilon_{ks} + i\eta} + \frac{T_{kk'}^{ss'*}}{\epsilon_{ks} - \epsilon_{k's'} + i\eta} \\ &+ \sum_{ps''} \frac{T_{kp}^{ss''} T_{k'p}^{s's''}}{(\epsilon_{ps''} - \epsilon_{ks} + i\eta)(\epsilon_{ps''} - \epsilon_{k's'} + i\eta)} \\ &= \delta_{kk'}\delta_{ss'}.\end{aligned} \tag{5.47}$$

Substituting the overlap eq. (5.46) into expression of the matrix element $X_{kk'}$, eq. (5.32), then we can find that

$$\begin{aligned}X_{kk'} &= \sum_{ps} \left(\delta_{pk}\delta_{s-} + \frac{T_{kp}^{s-}}{\epsilon_{ps} - \epsilon_{k-} + i\eta}\right)\left(\delta_{k'p}\delta_{s-} + \frac{T_{k'p}^{s-}}{\epsilon_{ps} - \epsilon_{k'-} + i\eta}\right) \\ &\times \left(1 - \mathrm{e}^{-i(\epsilon_{ps} - \epsilon_{k-})t/\hbar}\right) \\ &= \frac{T_{kk'}^{--}}{\epsilon_{k'-} - \epsilon_{k-} + i\eta}\left(1 - e^{-i(\epsilon_{k'-} - \epsilon_{k-})t/\hbar}\right) + \sum_{ps} \frac{T_{kp}^{s-}}{\epsilon_{ps} - \epsilon_{k-} + i\eta} \\ &\times \frac{T_{k'p}^{s-}}{\epsilon_{ps} - \epsilon_{k'-} + i\eta}\left(1 - e^{-i(\epsilon_{ps} - \epsilon_{k-})t/\hbar}\right)\end{aligned} \tag{5.48}$$

Using the unitary condition of the overlap tensor, we can express it in another form.

$$\begin{aligned}X_{kk'} &= -\left(\frac{T_{kk'}^{--*}}{\epsilon_{k-} - \epsilon_{k'-} + i\eta} + \sum_{ps} \frac{T_{kp}^{s-} T_{k'p}^{s-}}{(\epsilon_{ps} - \epsilon_{k-} + i\eta)(\epsilon_{ps} - \epsilon_{k'-} + i\eta)}\right) \\ &\times \left(1 - e^{-i(\epsilon_{k'-} - \epsilon_{k-})t/\hbar}\right) + \sum_{ps} \frac{T_{kp}^{s-} T_{k'p}^{s-}}{(\epsilon_{ps} - \epsilon_{k-} + i\eta)(\epsilon_{ps} - \epsilon_{k'-} + i\eta)} \\ &\times \left(1 - e^{-i(\epsilon_{ps} - \epsilon_{k-})t/\hbar}\right)\end{aligned} \tag{5.49}$$

In the large time limit, the last two terms cancel with each other so that one can cast the X matrix element into a simple way.

$$X_{kk'} = -\frac{T_{kk'}^{--*}}{\epsilon_{k-} - \epsilon_{k'-} + i\eta}\left(1 - e^{-i(\epsilon_{k'-} - \epsilon_{k-})t/\hbar}\right) \tag{5.50}$$

It is the same as the previous result. For intrinsic graphene, the Hamiltonian in the coordinate representation takes the following form.

$$H_0 = -i\hbar v_F \vec{\nabla} \cdot \vec{\sigma} \tag{5.51}$$

Its eigenstate is

$$\phi_{ks}(\vec{r}) = \frac{e^{i\tilde{k}\tilde{r}}}{\sqrt{2A}} \begin{pmatrix} 1 \\ se^{i\theta_k} \end{pmatrix} \tag{5.52}$$

In a polar coordinate system, the Dirac equation of electrons in the graphene can be written as

$$-i\hbar v_F \begin{pmatrix} 0 & e^{-i\varphi}(\partial_r - \frac{i}{r}\partial_\varphi) \\ e^{i\varphi}(\partial_r + \frac{i}{r}\partial_\varphi) & 0 \end{pmatrix} \psi(r,\phi) = E\psi(r,\varphi), \tag{5.53}$$

where $\varphi = \arctan(y/x)$. Thus, We can also express the eigen wave function in the cylindrical representation.

$$\phi_{ks}(r,\varphi) = \sum_l \frac{i^l}{\sqrt{2A}} \begin{pmatrix} J_l(kr)e^{il\varphi}e^{-il\theta_k} \\ isJ_{l+1}(kr)e^{i(l+1)\varphi}e^{-il\theta_k} \end{pmatrix} \tag{5.54}$$

The Bessel function satisfies the following radial differential equations.

$$\frac{dJ_{l+1}(kr)}{dr} + \frac{l+1}{r}J_{l+1}(kr) = kJ_l(kr) \tag{5.55}$$

$$\frac{dJ_l(kr)}{dr} - \frac{l}{r}J_l(kr) = -kJ_{l+1}(kr) \tag{5.56}$$

If we consider a central potential $V(r)$, the Hamiltonian becomes

$$\overline{H} = -i\hbar v_F \vec{\nabla} \cdot \vec{\sigma} + V(r) \tag{5.57}$$

Its eigenstate is the scattering wave function, and it generally takes the form,

$$\Psi_{ps}(r,\varphi) = \sum_l \frac{i^l \exp(i\delta_{ls})}{\sqrt{2A}} \begin{pmatrix} F_{ls}(pr)e^{il\varphi}e^{-il\theta_p} \\ iG_{ls}(pr)e^{i(l+1)\varphi}e^{-il\theta_p} \end{pmatrix}, \tag{5.58}$$

where $\theta_p = \arctan(p_y/p_x)$. $F_l(pr)$ and $G_l(pr)$ obey the radial differential equations [57].

$$\frac{dF_{ls}(pr)}{dr} - \frac{l}{r}F_{ls}(pr) + \frac{(\epsilon_{ps} - V(r))}{\hbar v_F}G_{ls}(pr) = 0 \tag{5.59}$$

$$\frac{dG_{ls}(pr)}{dr} + \frac{l+1}{r}G_{ls}(pr) - \frac{(\epsilon_{ps} - V(r))}{\hbar v_F}F_{ls}(pr) = 0 \tag{5.60}$$

From eq. (5.54) and eq. (5.58), one can find the T matrix.

$$T_{kp}^{s-} = \sum_l 2\pi \int_0^\infty \frac{(rJ_l(kr)V(r)F_{ls}(pr) - rJ_{l+1}(kr)V(r)G_{ls}(pr))dr}{2A} e^{il(\theta_k - \theta_p)} e^{i\delta_{ls}} \tag{5.61}$$

Version of July 12, 2021– Created July 12, 2021 - 12:37

Multiplying both sides of the eq. (5.59) and the eq. (5.60) by $rJ_{l+1}(kr)$ and $rJ_l(kr)$, respectively, we can get

$$\begin{aligned}
&rJ_{l+1}(kr)\frac{dF_{ls}(pr)}{dr} - \frac{l}{r}rJ_{l+1}(kr)F_{ls}(pr) + \frac{(\epsilon_{ps}-V(r))}{\hbar v_F}rJ_{l+1}(kr)G_{ls}(pr) \\
&= \frac{d[rJ_{l+1}(kr)F_{ls}(pr)]}{dr} - F_{ls}(pr)\left[r\frac{dJ_{l+1}(kr)}{dr} + (l+1)J_{l+1}(kr)\right] + \frac{(\epsilon_{ps}-V(r))}{\hbar v_F} \\
&\times rJ_{l+1}(kr)G_{ls}(pr) \\
&= \frac{d[rJ_{l+1}(kr)F_{ls}(pr)]}{dr} - krJ_l(kr)F_{ls}(pr) + \frac{(\epsilon_{ps}-V(r))}{\hbar v_F}rJ_{l+1}(kr)G_{ls}(pr) = 0.
\end{aligned} \tag{5.62}$$

$$\begin{aligned}
&rJ_l(kr)\frac{dG_{ls}(pr)}{dr} + \frac{l+1}{r}rJ_l(kr)G_{ls}(pr) - \frac{(\epsilon_{ps}-V(r))}{\hbar v_F}rJ_l(kr)F_{ls}(pr) \\
&= \frac{d[rJ_l(kr)G_{ls}(pr)]}{dr} - G_{ls}(pr)\left[r\frac{dJ_l(kr)}{dr} - lJ_l(kr)\right] - \frac{(\epsilon_{ps}-V(r))}{\hbar v_F}rJ_l(kr)F_{ls}(pr) \\
&= \frac{d[rJ_l(kr)G_{ls}(pr)]}{dr} + krJ_{l+1}(kr)G_{ls}(pr) - \frac{(\epsilon_{ps}-V(r))}{\hbar v_F}rJ_l(kr)F_{ls}(pr) = 0
\end{aligned} \tag{5.63}$$

After some algebra calculation, one can find

$$\begin{aligned}
T_{kp}^{s-} = -\sum_l \frac{\pi\hbar v_F}{A}\int_0^\infty \{&\frac{d[rJ_{l+1}(kr)F_{ls}(pr)]}{dr} + \frac{d[rJ_l(kr)G_{ls}(pr)]}{dr} \\
&+ (sp+k)\,rJ_{l+1}(kr)G_{ls}(pr) - (sp+k)\,rJ_l(kr)F_{ls}(pr)\}dr \\
&\times \exp[il(\theta_k-\theta_p)]\exp(i\delta_{ls})
\end{aligned} \tag{5.64}$$

At the large argument, the radial functions have the asymptotic forms as

$$J_l(kr) \simeq \sqrt{\frac{2}{\pi kr}}\cos\left(kr - \frac{l}{2}\pi - \frac{\pi}{4}\right) \tag{5.65}$$

$$F_{ls}(pr) \simeq \sqrt{\frac{2}{\pi pr}}\cos\left(pr - \frac{l}{2}\pi - \frac{\pi}{4} - \alpha s\ln(2pr) + \delta_{ls}\right) \tag{5.66}$$

$$G_l(pr) \simeq s\sqrt{\frac{2}{\pi pr}}\sin\left(pr - \frac{l}{2}\pi - \frac{\pi}{4} - \alpha s\ln(2pr) + \delta_{ls}\right) \tag{5.67}$$

The energy level of the helium ion is much greater than the energy of electrons, so elastic scattering dominates our calculation. In that case, $s = -$, and $p = K$, so we can find the T matrix.

$$\begin{aligned}
T_{kp}^{--} &= -\sum_l \frac{2\pi\hbar v_F}{\pi k A}[\sin\left(kr - \frac{l}{2}\pi - \frac{\pi}{4}\right) \\
&\times \cos\left(kr - \frac{l}{2}\pi - \frac{\pi}{4} + \delta_{l-} + \alpha\ln(2kr)\right) - \cos\left(kr - \frac{l}{2}\pi - \frac{\pi}{4}\right) \\
&\times \sin\left(kr - \frac{l}{2}\pi - \frac{\pi}{4} + \delta_{l-} + \alpha\ln(2kr)\right)]e^{il(\theta_k-\theta_p)}e^{i\delta_{l-}} \\
&= \sum_l \frac{2\pi\hbar v_F}{\pi k A}e^{il(\theta_k-\theta_p)}\exp(-i\alpha\ln(2kr))\frac{\exp(2i\delta_{l-} + 2i\alpha\ln(2kr)) - 1}{2i} \\
&= \sum_l \frac{e^{il(\theta_k-\theta_p)}}{\pi\nu(k)}\exp(-i\alpha\ln(2kr))[\exp(2i\alpha\ln(2kr))\frac{\exp(2i\delta_{l-}) - 1}{2i} \\
&+ \frac{\exp(2i\alpha\ln(2kr)) - 1}{2i}]
\end{aligned} \tag{5.68}$$

r is the screened radius of Coulomb potential, which is extended to infinity for pure Coulomb potential. The last term in the bracket is independent on l so that one can write the T matrix as,

$$\begin{aligned}
T_{kp}^{--} &= \sum_l \frac{e^{il(\theta_k-\theta_p)}}{\pi\nu(k)}\exp(i\alpha\ln(2kr))\frac{\exp(2i\delta_{l-}) - 1}{2i} \\
&+ \frac{\exp(i\alpha\ln(2kr)) - \exp(-i\alpha\ln(2kr))}{i\nu(k)}\delta(\theta_k - \theta_p),
\end{aligned} \tag{5.69}$$

$\nu(k)$ is the density of state. Here we use the formula,

$$\sum_l e^{il(\theta_k-\theta_p)} = 2\pi\delta(\theta_k - \theta_p). \tag{5.70}$$

Notice that the second term is only nonzero if $\theta_k = \theta_p$, so one can neglect the second term when $\theta_k \neq \theta_p$. Moreover, the factor $\exp(i\alpha\ln(2kr))$ is insignificant because the T matrix and its conjugate show in pair in our problem. Therefore, the T matrix recovers to the standard expression when $\theta_k \neq \theta_p$,

$$T_{kp}^{--} = \sum_l \frac{e^{il(\theta_k-\theta_p)}}{\pi\nu(k)}\exp(i\delta_{l-})\sin\delta_{l-}. \tag{5.71}$$

Version of July 12, 2021– Created July 12, 2021 - 12:37

For the inter-band scattering, s=+, the calculation is the same as in the eq. (5.68), so we do not repeat it again and only give the result that the T matrix vanishes at a large distance. Eq. (5.68) gives the same result as before. For the lowest scattering channel, from eq. (5.50), one can obtain that the X matrix element.

$$X_{kk'} = \frac{\exp(-i\delta_-)\sin\delta_-}{\pi\nu(k)(\epsilon_k - \epsilon_{k'} - i\eta)}\left(1 - e^{i(\epsilon_{k'}-\epsilon_k)t/\hbar}\right) \tag{5.72}$$

Bibliography

[1] A. A. Penzias and R. W. Wilson, *A Measurement of Excess Antenna Temperature at 4080 Mc/s.*, Astrophysical Journal **142**, 419 (1965).

[2] C. L. Bennett et al., *Nine-year Wilkinson Microwave Anisotropy Probe (WMAP) observations: final maps and results*, The Astrophysical Journal Supplement Series **208**, 20 (2013).

[3] Planck Collaboration et al., *Planck 2013 results. V. LFI calibration*, Astronomy & Astrophysics **571**, A5 (2014).

[4] Y. F. Li, Z.-z. Xing, and S. Luo, *Direct detection of the cosmic neutrino background including light sterile neutrinos*, Physics Letters B **692**, 261 (2010).

[5] K. Collaboration, *KATRIN design report 2004*, Wissenschaftliche Berichte FZKA **7090** (2005).

[6] F. L. Wilson, *Fermi's theory of beta decay*, American Journal of Physics **36**, 1150 (1968).

[7] L. I. Bodine, D. S. Parno, and R. G. H. Robertson, *Assessment of molecular effects on neutrino mass measurements from tritium β decay*, Physical Review C **91**, 035505 (2015).

[8] A. G. Cocco, G. Mangano, and M. Messina, *Probing low energy neutrino backgrounds with neutrino capture on beta decaying nuclei*, Journal of Cosmology and Astroparticle Physics **2007**, 015 (2007).

[9] S. Betts et al., *Development of a relic neutrino detection experiment at PTOLEMY: princeton tritium observatory for light, early-universe, massive-neutrino yield*, arXiv preprint arXiv:1307.4738 (2013).

[10] A. Faessler, R. Hodak, S. Kovalenko, and F. Å imkovic, *Beta Decay and the Cosmic Neutrino Background*, EPJ Web of Conferences **71**, 00044 (2014).

[11] B. Monreal and J. A. Formaggio, *Relativistic cyclotron radiation detection of tritium decay electrons as a new technique for measuring the neutrino mass*, Physical Review D **80**, 051301 (2009).

[12] E. Baracchini et al., *PTOLEMY: A proposal for thermal relic detection of massive neutrinos and directional detection of MeV dark matter*, arXiv preprint arXiv:1808.01892 (2018).

[13] M. Betti et al., *Neutrino physics with the PTOLEMY project: active neutrino properties and the light sterile case*, Journal of Cosmology and Astroparticle Physics **2019**, 047 (2019).

[14] Y. V. Skrypnyk and V. M. Loktev, *Metal-insulator transition in hydrogenated graphene as manifestation of quasiparticle spectrum rearrangement of anomalous type*, Physical Review B **83**, 085421 (2011).

[15] Y. Hochberg, Y. Kahn, M. Lisanti, C. G. Tully, and K. M. Zurek, *Directional detection of dark matter with two-dimensional targets*, Physics Letters B **772**, 239 (2017).

[16] K. Ohtaka and Y. Tanabe, *Theory of the soft-x-ray edge problem in simple metals: historical survey and recent developments*, Reviews of Modern Physics **62**, 929 (1990).

[17] P. W. Anderson, *Infrared Catastrophe in Fermi Gases with Local Scattering Potentials*, Physical Review Letters **18**, 1049 (1967).

[18] A. Kramida, Yu. Ralchenko, J. Reader, and and NIST ASD Team, NIST Atomic Spectra Database (ver. 5.8), [Online]. Available: `https://physics.nist.gov/asd` [2021, July 11]. National Institute of Standards and Technology, Gaithersburg, MD., 2020.

[19] M. Bonfanti, S. Achilli, and R. Martinazzo, *Sticking of atomic hydrogen on graphene*, Journal of Physics: Condensed Matter **30**, 283002 (2018).

[20] H. González-Herrero, E. Cortés-del Río, P. Mallet, J. Veuillen, J. Palacios, J. Gómez-Rodríguez, I. Brihuega, and F. Ynduráin, *Hydrogen physisorption channel on graphene: a highway for atomic H diffusion*, 2D Materials **6**, 021004 (2019).

[21] D. Chitwood et al., *Improved measurement of the positive-muon lifetime and determination of the Fermi constant*, Physical review letters **99**, 032001 (2007).

[22] B. Roulet, J. Gavoret, and P. Nozières, *Singularities in the X-Ray Absorption and Emission of Metals. I. First-Order Parquet Calculation*, Physical Review **178**, 1072 (1969).

[23] P. Nozières, J. Gavoret, and B. Roulet, *Singularities in the X-Ray Absorption and Emission of Metals. II. Self-Consistent Treatment of Divergences*, Physical Review **178**, 1084 (1969).

[24] M. Combescot and P. Nozières, *Infrared catastrophy and excitons in the X-ray spectra of metals*, Journal de Physique **32**, 913 (1971).

[25] G. D. Mahan, *Many-Particle Physics*, pages 90–94, 192–195, 325–335, 612–621, Physics of Solids and Liquids, Springer US, 3 edition, 2000.

[26] G. Mahan, *Many-body effects on x-ray spectra of metals*, in *Solid State Physics*, volume 29, pages 75–138, Elsevier, 1974.

[27] E. Kogan and M. Kaveh, *On the X-Ray Edge Problem in Graphene*, Graphene **7**, 1 (2018).

[28] P. Brouwer, *Theory of many particle system*, pages 100–105, unprinted, 2005.

[29] E. H. Hwang and S. Das Sarma, *Dielectric function, screening, and plasmons in two-dimensional graphene*, Physical Review B **75**, 205418 (2007).

[30] M. I. Katsnelson, *The Physics of Graphene*, pages 141–145,181–186, Cambridge University Press, 2 edition, 2020.

[31] K. W. K. Shung, *Dielectric function and plasmon structure of stage-1 intercalated graphite*, Physical Review B **34**, 979 (1986).

[32] Y. Cheipesh, V. Cheianov, and A. Boyarsky, *Heisenberg's uncertainty as a limiting factor for neutrino mass detection in β-decay*, arXiv preprint arXiv:2101.10069 (2021).

[33] G. Giuliani and G. Vignale, *Quantum theory of the electron liquid*, pages 177–181, Cambridge university press, 2005.

[34] D. Gall, *Electron mean free path in elemental metals*, Journal of Applied Physics **119**, 085101 (2016).

[35] J. Sólyom, *Fundamentals of the Physics of Solids: Volume 3 - Normal, Broken-Symmetry, and Correlated Systems*, pages 98–99, Theoretical Solid State Physics: Interaction Among Electrons, Springer Berlin Heidelberg, 2010.

[36] B. Mihaila, *Lindhard function of a d-dimensional Fermi gas*, arXiv preprint arXiv:1111.5337 (2011).

[37] N. D. Mermin, *Lindhard Dielectric Function in the Relaxation-Time Approximation*, Physical Review B **1**, 2362 (1970).

[38] D. Pines, *Theory of Quantum Liquids: Normal Fermi Liquids*, pages 10–12, 159–162, CRCP ress, 2018.

[39] Y. Chen and J. Kroha, *X-ray-photoemission spectra of impure simple metals*, Physical Review B **46**, 1332 (1992).

[40] F. Giannazzo, S. Sonde, R. L. Nigro, E. Rimini, and V. Raineri, *Mapping the density of scattering centers limiting the electron mean free path in graphene*, Nano letters **11**, 4612 (2011).

[41] L. Banszerus, M. Schmitz, S. Engels, M. Goldsche, K. Watanabe, T. Taniguchi, B. Beschoten, and C. Stampfer, *Ballistic transport exceeding 28 µm in CVD grown graphene*, Nano letters **16**, 1387 (2016).

[42] M. Moaied, J. Moreno, M. Caturla, F. Ynduráin, and J. Palacios, *A theoretical study of the dynamics of atomic hydrogen on graphene bilayers*, arXiv preprint arXiv:1405.3165 (2014).

[43] F. Ding and B. I. Yakobson, *Challenges in hydrogen adsorptions: from physisorption to chemisorption*, Frontiers of Physics **6**, 142 (2011).

[44] T. Stauber, N. M. R. Peres, and F. Guinea, *Electronic transport in graphene: A semiclassical approach including midgap states*, Physical Review B **76**, 205423 (2007).

[45] M. Hentschel and F. Guinea, *Orthogonality catastrophe and Kondo effect in graphene*, Physical Review B **76**, 115407 (2007).

[46] D. M. Basko, *Resonant low-energy electron scattering on short-range impurities in graphene*, Physical Review B **78**, 115432 (2008).

[47] G. Canright, *Time-dependent screening in the electron gas*, Physical Review B **38**, 1647 (1988).

[48] F. Bornemann, *On the numerical evaluation of Fredholm determinants*, Mathematics of Computation **79**, 871 (2010).

[49] B. Simon, *Trace ideals and their applications*, pages 45–52, Number 120 in Mathematical surveys and monographs, American Mathematical Soc., 2005.

[50] P. NOzières and C. T. De Dominicis, *Singularities in the X-Ray Absorption and Emission of Metals. III. One-Body Theory Exact Solution*, Physical Review **178**, 1097 (1969).

[51] J. J. Sakurai and J. Napolitano, *Modern Quantum Mechanics*, pages 411–414, Cambridge University Press, 2 edition, 2017.

[52] S. K. Adhikari, *Quantum scattering in two dimensions*, American Journal of Physics **54**, 362 (1986).

[53] N. W. Ashcroft et al., *Solid state physics*, volume 2005, holt, rinehart and winston, new york London, 1976.

[54] T. Ando, *Screening Effect and Impurity Scattering in Monolayer Graphene*, Journal of the Physical Society of Japan **75**, 074716 (2006).

[55] E. H. Hwang, S. Adam, and S. D. Sarma, *Carrier Transport in Two-Dimensional Graphene Layers*, Physical Review Letters **98**, 186806 (2007).

[56] S. Adam, *Graphene Carrier Transport Theory*, in *Graphene Nanoelectronics*, pages 357–394, Springer Berlin Heidelberg, 2011.

[57] D. S. Novikov, *Elastic scattering theory and transport in graphene*, Physical Review B **76**, 245435 (2007).

[58] V. M. Pereira, J. Nilsson, and A. H. Castro Neto, *Coulomb Impurity Problem in Graphene*, Physical Review Letters **99**, 166802 (2007).

[59] A. V. Shytov, M. I. Katsnelson, and L. S. Levitov, *Vacuum Polarization and Screening of Supercritical Impurities in Graphene*, Physical Review Letters **99**, 236801 (2007).

[60] J. Kunc and M. Rejhon, *Raman 2D Peak Line Shape in Epigraphene on SiC*, Applied Sciences **10**, 2354 (2020).

[61] A. H. Castro Neto, F. Guinea, N. M. R. Peres, K. S. Novoselov, and A. K. Geim, *The electronic properties of graphene*, Reviews of Modern Physics **81**, 109 (2009).

[62] B. Schneider, *Some notes on the Poincaré-Bertrand formula*, Journal of Applied Mathematics **2012** (2012).

Version of July 12, 2021– Created July 12, 2021 - 12:37